SUPPORTING INFORMATION

Genesis of MoS_2 from model-Mo-oxide precursors supported on γ-alumina

*Amit Sahu, [†§] Stephan N. Steinmann,[§] and Pascal Raybaud[†§]**

[†] IFP Energies nouvelles, Direction Catalyse et Séparation, Rond-Point de l'Échangeur de Solaize, BP 3, 69360 Solaize, France.

[§] Univ Lyon, ENS de Lyon, CNRS, Université Claude Bernard Lyon 1, Laboratoire de Chimie UMR 5182, F-69342 Lyon, France.

Contents

1. Computational details

1.1 Adsorption energy

For determining the adsorption energy (ΔE) of the starting Mo_nO_{3n} (n=1 to 3) oxides oligomers on alumina at 0 K, the following equation was used:

$$\gamma - \mathbf{Al_2O_3} + \mathbf{n} \times \mathbf{MoO_{3(bulk)}} \rightarrow \mathbf{Mo_nO_{3n}}@\gamma - \mathbf{Al_2O_3} \qquad \textbf{SE1}$$

$$\mathbf{\Delta E} = \frac{\mathbf{1}}{\mathbf{n}}\left[\mathbf{E(Mo_nO_{3n}}@\gamma - \mathbf{Al_2O_3}) - \mathbf{n} \times \mathbf{E}\left(\mathbf{MoO_{3(bulk)}}\right) - \mathbf{E}(\gamma - \mathbf{Al_2O_3})\right] \qquad \textbf{SE2}$$

where $E(Mo_nO_{3n}@\gamma - Al_2O_3)$ is the electronic energy of the adsorbed Mo_nO_{3n} oligomers (n=1, 2 and 3), $E(MoO_3)$ is the energy of bulk-MoO_3 and $E(\gamma - Al_2O_3)$, the energy of the γ–alumina (100) slab representing the surface.

To determine the O/S exchange thermochemistry energy at 0K, which occurs through H_2S adsorption either on oxide-cluster or support, we used the following equation:

$$\mathbf{Mo_nO_{3n}}@\gamma - \mathbf{Al_2O_3} + \mathbf{xH_2S} \rightarrow \mathbf{Mo_nO_{3n-x}S_x}@\gamma - \mathbf{Al_2O_3} + \mathbf{xH_2O} \qquad \textbf{SE3}$$

$$\mathbf{\Delta E} = [\mathbf{E(Mo_nO_{3n-x}S_x}@\gamma - \mathbf{Al_2O_3}) + \mathbf{xE(H_2O)} - \mathbf{E(Mo_nO_{3n}}@\gamma - \mathbf{Al_2O_3}) - \mathbf{xE(H_2S)}] \qquad \textbf{SE4}$$

where $E(Mo_nO_{3n-x}S_x@\gamma - Al_2O_3)$ is the energy of alumina supported Mo-oxysulfide after x number of O/S exchanges, $E(H_2O)$ is the energy of water, $E(Mo_nO_{3n}@\gamma - Al_2O_3)$ is the energy of alumina supported Mo-oxide, and $E(H_2S)$ is the energy of H_2S. To calculate the energy change during a single O/S exchange, we have used the following equation:

$$\boldsymbol{Mo_nO_{3n-x}S_x}@\gamma - \mathbf{Al_2O_3} + \boldsymbol{H_2S} \rightarrow \boldsymbol{Mo_nO_{3n-x-1}S_{x+1}}@\gamma - \mathbf{Al_2O_3} + \boldsymbol{H_2O} \qquad \textbf{SE5}$$

$$\mathbf{\Delta E = E(Mo_nO_{3n-x-1}S_{x+1}@\gamma - Al_2O_3) + E(H_2O) - E(Mo_nO_{3n-x}S_x@\gamma - Al_2O_3) - E(H_2S)} \quad \mathbf{SE6}$$

The reaction energy of the O-removal (reduction) on $Mo_nO_nS_{2n}$ oxysulfides or Mo_nS_{3n} trisulfides occurring under H_2 (g), was calculated according to :

$$\mathbf{Mo_nO_{n-x}S_{2n}@\gamma - Al_2O_3 + H_2 \rightarrow Mo_nO_{n-x-1}S_{2n} \ @\gamma - Al_2O_3 + H_2O} \quad \mathbf{SE7}$$

$$\mathbf{\Delta E = \left[E\left(Mo_nO_{n-x-1}S_{2n} \ @\gamma - Al_2O_3\right) + E(H_2O) - E(Mo_nO_{n-x}S_{2n}@\gamma - Al_2O_3) - E(H_2)\right]} \quad \mathbf{SE8}$$

where $E\left(Mo_nO_{n-x-1}S_{2n} \ @\gamma - Al_2O_3\right)$ is the energy of γ–alumina supported $Mo_nO_{n-x-1}S_{2n}$ intermediate oxysulfides.

The underlying assumption is that the reduction of oxysulfide starts when it reaches a S/Mo stoichiometry of 2. This assumption is based on our observation of the endothermic process of water removal from pure oxides by using H_2.

Similarly, for the S-removal on trisulfide (Mo_nS_{3n}) to lead to Mo-disulfide oligomers (Mo_nS_{2n}) by H_2:

$$\mathbf{Mo_nS_{3n-x}@\gamma - Al_2O_3 + H_2 \rightarrow Mo_nS_{3n-x-1} \ @\gamma - Al_2O_3 + H_2S} \quad \mathbf{SE9}$$

$$\mathbf{\Delta E = \begin{bmatrix} E\left(Mo_nS_{3n-x-1} \ @\gamma - Al_2O_3\right) + E(H_2S) \\ -E(Mo_nS_{3n-x}@\gamma - Al_2O_3) - E(H_2) \end{bmatrix}} \quad \mathbf{SE10}$$

where, $E\left(Mo_nS_{3n-x-1} \ @\gamma - Al_2O_3\right)$ is the energy of supported Mo_nS_{3n-x-1} oligomer and $E(Mo_nS_{3n-x}@\gamma - Al_2O_3)$ is the energy of Mo_nS_{3n-x} oligomers.

1.2 Slab model of alumina (100) surface

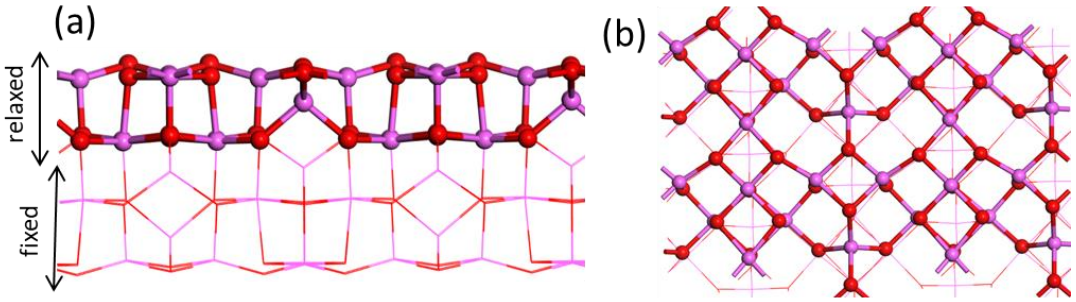

Figure S1. Molecular model of the (100) surface of γ-alumina[1,2]. a) side view and b) top view of the surface. Balls and sticks represent the movable slab, and lines represent the fixed slab. (Color legend: red balls: O, pink balls: Al).

1.3 Thermodynamic corrections for gas phase molecules

In order to evaluate the free energies associated to adsorption and desorption steps of the H_2, H_2S and H_2O molecules, we considered that they keep all vibrational, rotational and translational degrees of freedom in gas phase. Thus, the corresponding ZPE, H(T) and S(T) terms are determined by using the partition functions applied to diatomic (H_2) and triatomic (H_2S and H_2O) molecules as provided in Ref. [3]

To calculate numerically the rotational and translational entropies at 625 K, we used this online tool https://www.colby.edu/chemistry/PChem/scripts/ABC.html by providing the optimized geometry coordinates. At 625 K, the computed rotational plus translational free energies of H_2, H_2S, and H_2O are 0.80 eV, 1.17 eV, and 1.28 eV, respectively (to be added to the vibrational contributions).

Moreover, all diagrams reported in the main text assume $P = P_0$. An entropic term associated to the partial pressure of each ideal gas phase molecule with respect to standard P_0 should be added: $-Rln(P/P_0)$. It is thus possible to add the $RTln(P/P_0)$ corrective term on free energies of H_2, H_2S and H_2O in gas phase to be included during their adsorption or desorption

steps at a temperature of 625 K and for plausible partial pressures used during experimental sulfo-reduction:

- For H_2, $P(H_2)$ = 10 bar, the correction on free energy of H_2 adsorption is ΔG_{corr} = –0.12 eV,
- For H_2S, $P(H_2S)$ = 0.5 bar, the correction on free energy of H_2S adsorption is ΔG_{corr} = +0.04 eV (a negative value should be used for H_2S desorption steps)
- For H_2O, $P(H_2O)$ is not controlled during the sulfo-reductive process and it is actually endogenous. So, we assume that water partial pressure will remain low and increases slightly during the sulfidation process (in a plug flow reactor). As a rough approximation, for $0.01 \leq P(H_2O) \leq 0.1$ bar, the correction on free energy of desorption of water may be : $-0.25 \leq \Delta G_{corr} \leq -0.12$ eV.

From a practical use, in the free energy profiles reported in the main text or in Supporting information, the reader may thus use these corrective ΔG_{corr} values to shift the free energy levels of the starting states (reference free energy fixed at 0 eV) and of the final states, which correspond to adsorption and desorption steps, respectively.

2. Gas-phase analysis

2.1. Structural analysis

We have first performed the structural and thermodynamic analysis of monomer (Mo_1O_3), dimer (Mo_2O_6), and trimer (Mo_3O_9) in the gas phase. We analyzed their ground state structures and the relative stability of these oligomers concerning monomers (per Mo_1O_3).

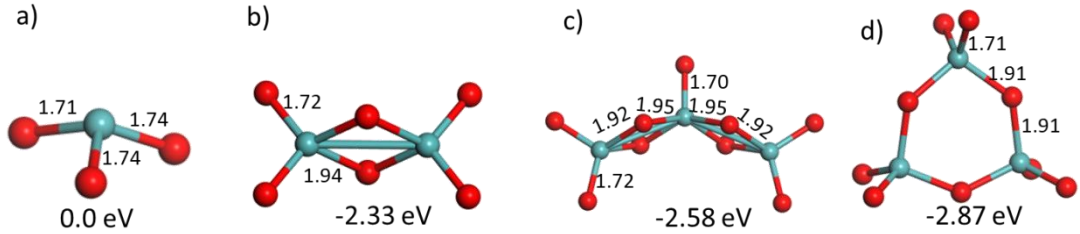

Figure S2. gas-phase structures of a) monomer (Mo_1O_3), b) dimer (Mo_2O_6), and c)-d) trimer (Mo_3O_9) chain and cyclic conformers.

2.2. Sulfidation in the gas phase

a) Dimer

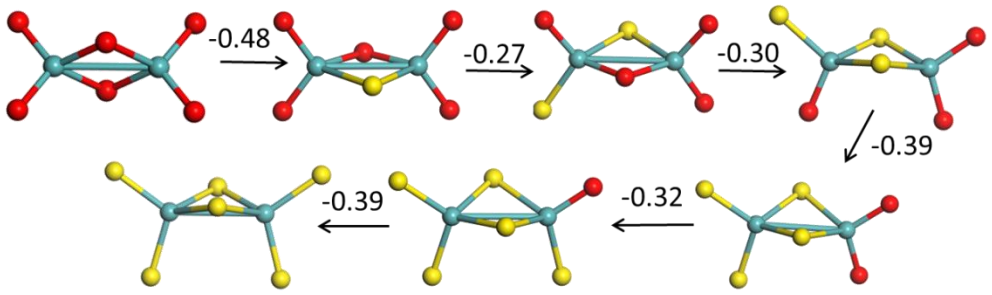

b) Cyclic-Trimer

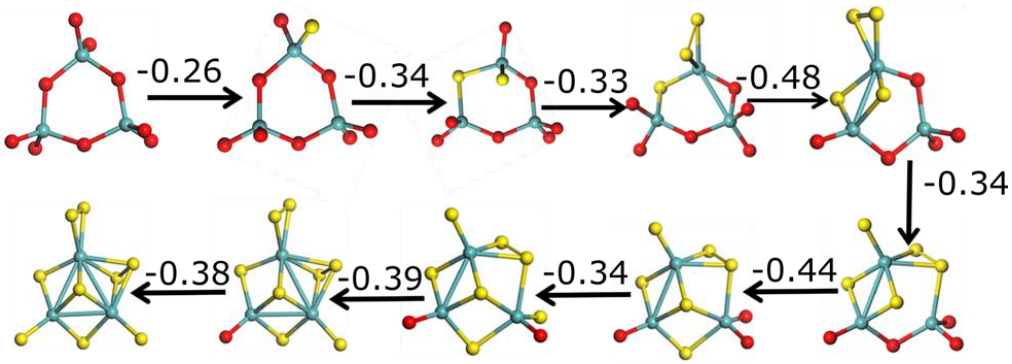

c) Chain-trimer

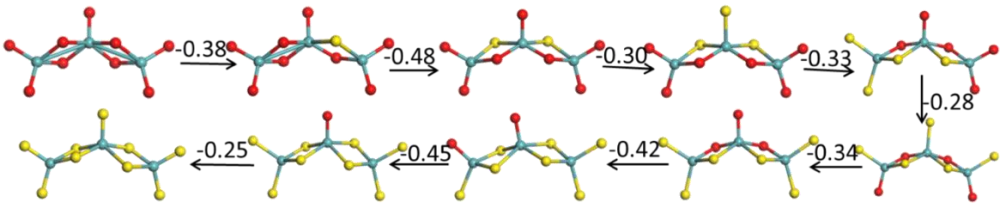

Figure S3. Sulfidation of various Mo-Oxides using H_2S/H_2O exchange: a) Dimer, b) Cyclic-trimer, c) chain-trimer.

2.3. Thermodynamics of gas-phase sulfidation

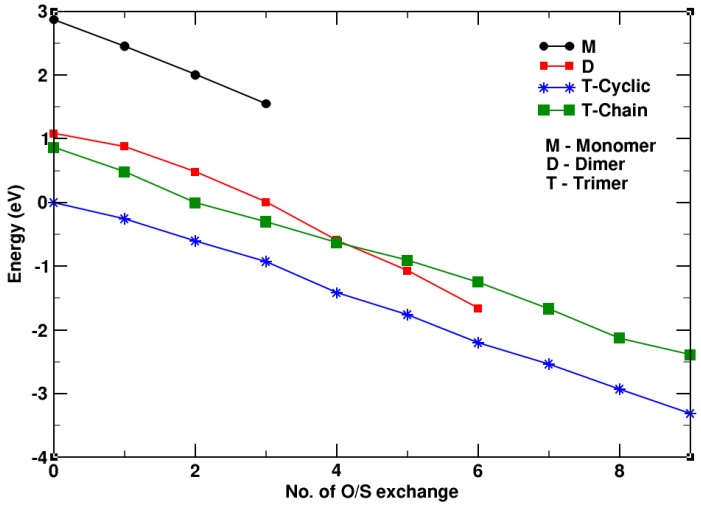

Figure S4. Thermodynamic energy diagram of sulfidation of monomer, dimer, and trimer (chain and cyclic) as a function of O/S exchange.

3. Alumina supported Mo-oxides

3.1. Monomer and Dimer

Handzlik and Sautet previously investigated monomeric and dimeric Mo oxides in interaction with γ-alumina using DFT with PW91-GGA exchange correlational functional without dispersion corrections.[4,5] We confirmed that the di-oxo Mo_1O_3 conformers adsorbed on (100) surface were found to be more stable by about 12 kJ.mol^{-1} than the mono-oxo one. However, the most stable adsorption site we found is different from the one reported by Handzlik and Sautet,[4] which may be due to an effect of dispersion corrections included in the present work. The energy difference between the two sites is about 0.25 eV in favor of our revised data. In our revised configuration, we find slightly shorter Mo-O-Al (1.83 Å vs. 1.86 Å[4]) and Mo-O_{surf} (1.98 Å vs. 2.16 Å[4]) bonds featuring much stronger interaction between Mo-oxides and surface (Figure S5a and b). For the dimeric species, we find the configuration illustrated in Figure S5c, very similar to the one reported by Handzlik et al.: one Mo-atom bearing a mono-oxo species and another Mo bearing a di-oxo. Moreover, the formation energy of the supported dimer (with respect to supported monomers) is also consistent (115 kJ/mol vs. 123[5] kJ/mol).

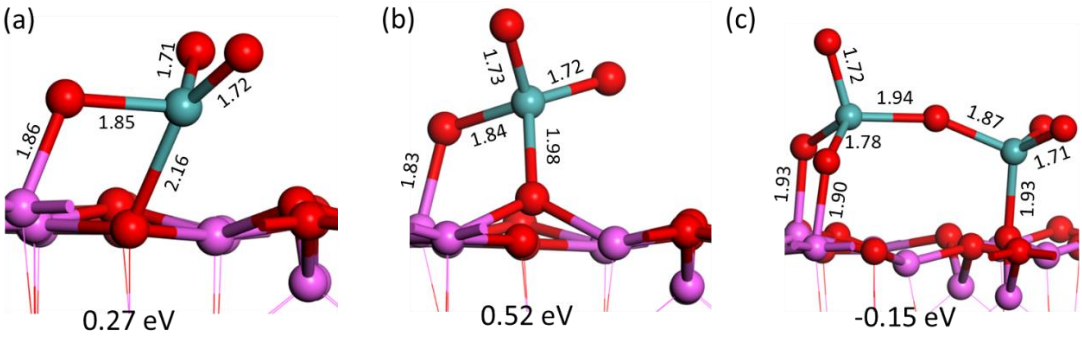

Figure S5. The most stable di-oxo conformers of Mo_1O_3 on alumina: a) most stable proposed by Handzlik and Sautet and b) most stable in this study, and c) conformers for Mo_2O_6. Bond lengths of various Mo-O and O-Al bonds are given in Å. The energy represented here is

relative to bulk MoO_3 and normalized to one formula unit (equation SE2). (Color code-Red: O, Pink: Al, and Blue: Mo).

The support has thus a significant impact on the relative stability and structures of these MoO_3 oligomers with respect to their gas-phase structures. For Mo_1O_3, Mo_2O_6, and Mo_3O_9 (chain, cyclic), Mo-atom prefers mainly a tetrahedral structure in the gas phase (except the central atom of the chain, which exhibits the square pyramidal shape in the gas phase). On the support, Mo_3O_9 chain-conformer exhibit two isoenergetic structures called chain-1 and chain-2.

3.2. Trimer

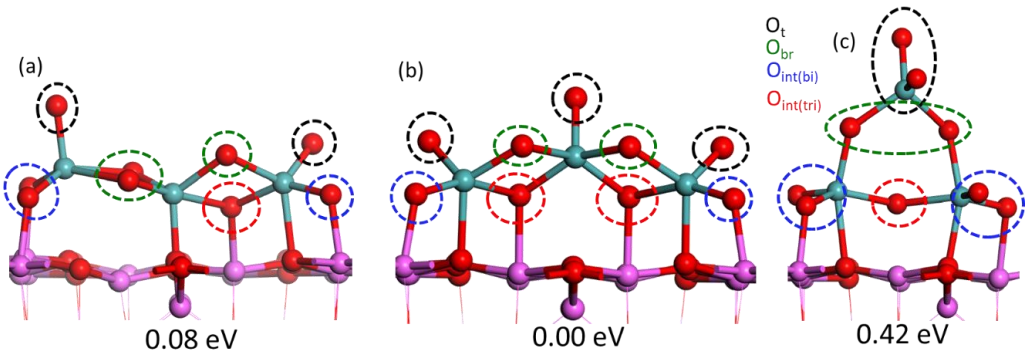

Figure S6. Most stable trimer (Mo_3O_9) on (100) surface of alumina: a) chain-1, b) chain-2, and c) cyclic conformers. (Red: O, Pink: Al, and Blue: Mo).

The most stable cyclic trimer structure is quite similar among the various conformers except for the local structure of the "central" Mo-atom located at a larger distance from the support. This central Mo-atom has a tetrahedral configuration, while the two other Mo-atoms are of distorted trigonal bipyramidal structure with 4 O ligands belonging to the cluster and one O to alumina. This cyclic trimer has two oxo species, two bridgings, four interfacial-bidentate, and

one interfacial-tridentate type of oxygens. The chain and triangular models exhibit the most stable conformer at the same adsorption site of alumina.

Table S1. Various types of oxygen observed in the system (notation and their respective description).

Notation	Description	Chain-1	Chain-2	Cyclic
O_t	Terminal oxo- singularly bonded to one Mo atom	2	3	2
O_{br}	Bridging oxo- bonded to two Mo (Mo-O-Mo)	3	2	2
$O_{int(bi)}$	Interfacial oxygen bonded to one Mo and one Al of alumina (Mo-O-Al)	3	2	4
$O_{int(tri)}$	Interfacial oxygen bonded to two Mo of cluster and on Al of support (Mo—O—Mo / Al)	1	2	1
O_{surf}	Oxygen from support interacting with Mo of the cluster	2	2	2

4. Supported monomer (Mo_1O_3) sulfidation

a) terminal

b) interfacial

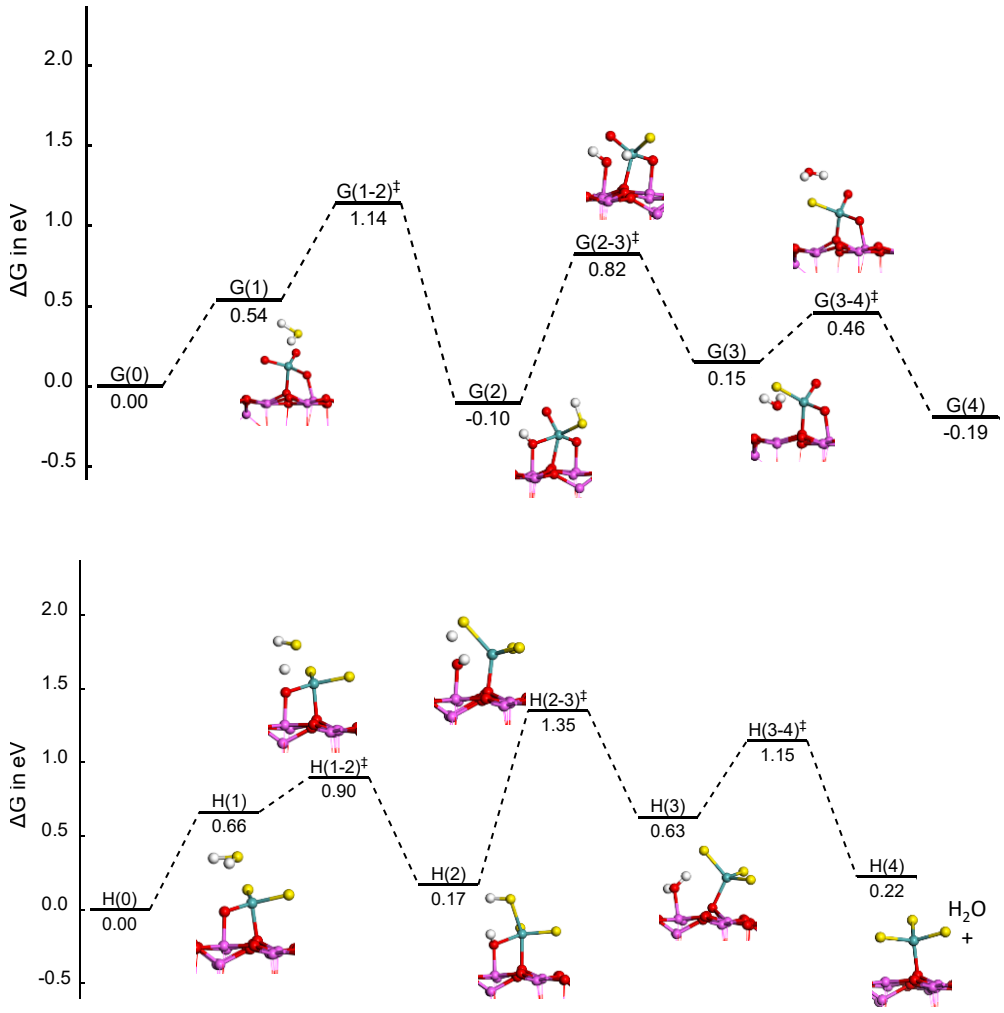

Figure S7. Mo-Oxides to Mo-sulfides transformation by O/S exchange ($MoO_3 \rightarrow MoS_3$) supported on alumina: a) bridging oxygen, b) terminal oxygen.

Gibb's free energy plot of O/S exchange for top-oxo of monomer has been shown in Figure S7 a. The dissociation of H_2S is the rate-limiting step that costs 1.14 eV. The formation of water and the desorption of water are the other critical steps in this reaction mechanism. Overall, the process is exothermic and thermodynamically favorable. We assume that the second oxo would also be replaced in a similar manner. We further investigated the interfacial oxygen in a monomer that has an activation energy of 1.35 eV. This requires transferring of the second proton from sulfur to oxygen. Overall, the O/S exchange is more favorable for the

monomer than the trimer due to the lower activation energy. Water desorption is the second most expensive step, as is the case for another interfacial oxygen.

5. Supported trimer (Mo_3O_9) sulfidation

5.1. Structural analysis of supported trimer (Mo_3O_9) sulfidation

a) Cyclic-trimer

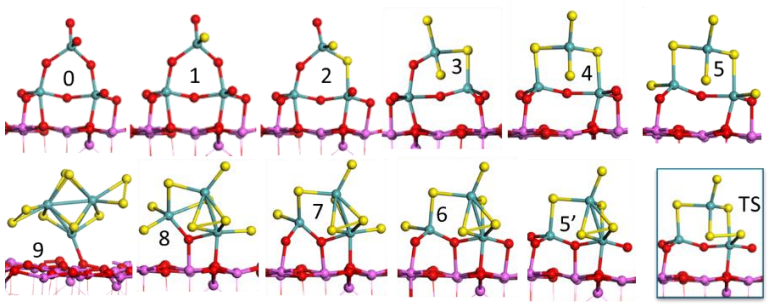

b) Chain-1 trimer path-1

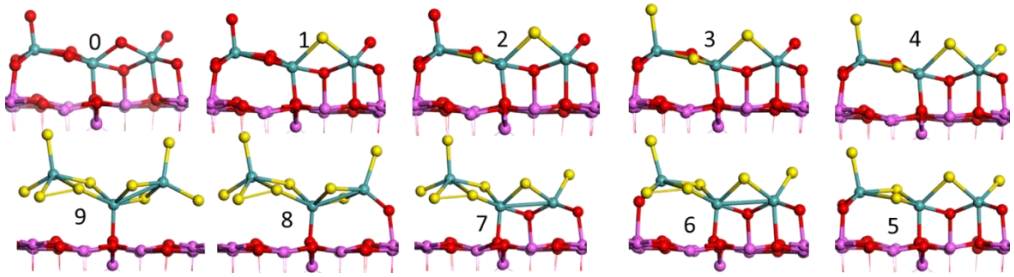

c) Chain-1 trimer path-2

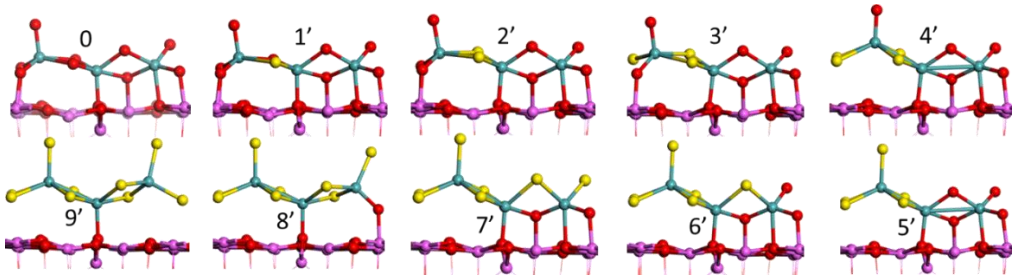

d) Chain-1 trimer combined

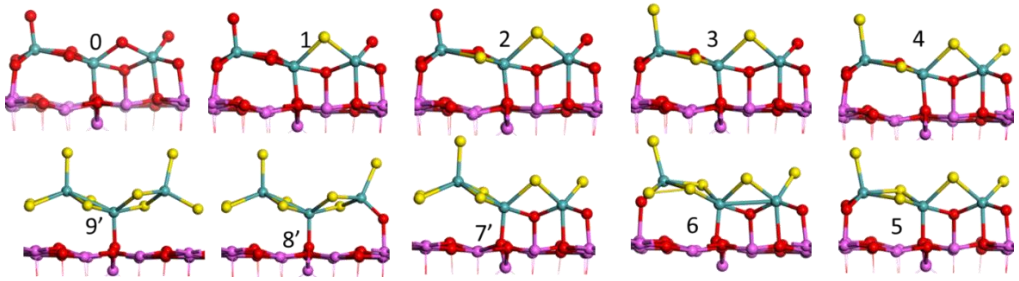

e) Chain-2 trimer

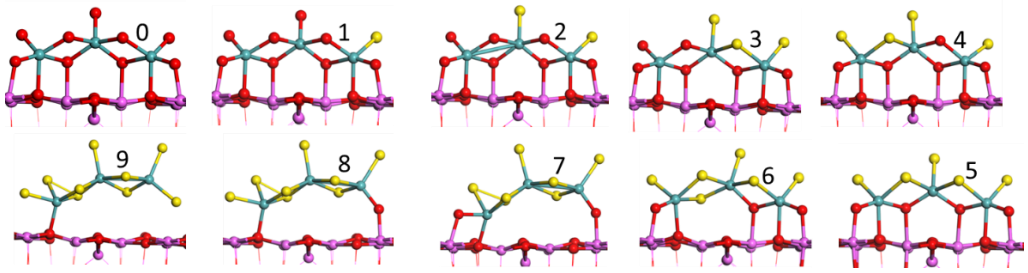

Figure S8. Mo-Oxides to Mo-sulfides transformation by O/S exchange (Mo_3O_9 → Mo_3S_9) supported on alumina: a) cyclic-trimer, b) chain-1 path-1, c) chain-1 path-2 d) chain-1-combined, e) chain-2.

Sulfidation of cyclic-Mo_3O_9 occurs similarly to chain-Mo_3O_9. The terminal and bridging oxygens are primarily the first ones to be replaced, followed by interfacial oxygens. The formation of dimers appeared after 5 O/S exchanges by costing the 0.5 eV of activation energy. Though the final Mo_3S_9 after all the O/S exchange is not the most stable one. The most stable supported TR-Mo_3S_9 is significantly different and needs various S diffusion to reach the most stable form.

5.2. EXAFS comparison and Simulated IR spectrum using DFPT

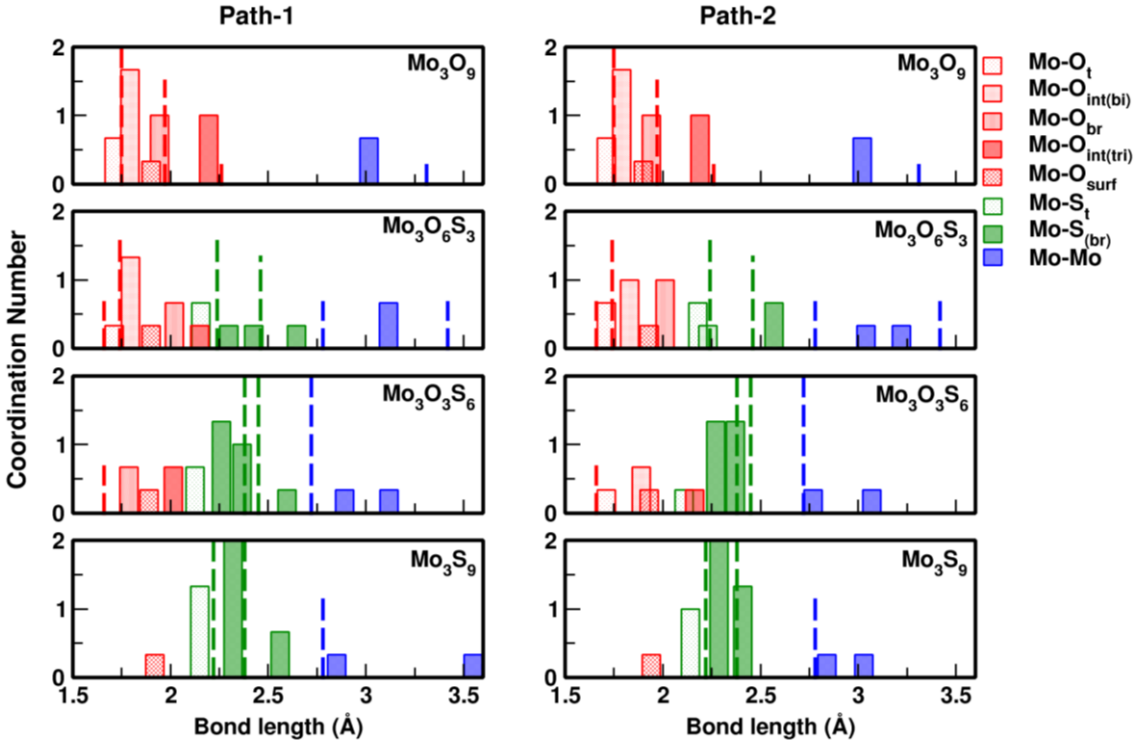

Figure S9. Evolution of various types of bond lengths and their coordination number for path-1 and path-2 during oxide to trisulfide sulfidation. Mo-O/Mo-S labels represent the majority of bonds belonging to the type of atom at a particular bond-length. The dashed lines represent the respective bond length with coordination number measured by EXAFS.[6]

Regarding the chain Mo-oxide species, the terminal oxo-site exhibits the shortest Mo-O_t bond (calculated at 1.71 Å vs. 1.74 Å experimentally)[6,7] and the interfacial-tridentate/bridging oxo-site (Mo-$O_{int\text{-}tri/br}$-Mo) reveals the longest bond at 2.10 Å (2.26 Å[8]) among all Mo-O bonds, while the interfacial-bidentate oxygens (Mo-O-(Al) and Mo-O_{surf}) have an intermediate bond length around 1.86-2.28 Å (1.96Å [6]). No short Mo-Al bond is found for Mo-oxide species as reported by some EXAFS data,[7–9] but we recovered the long Mo-Al bond of 3.06 Å (3.06 Å[6,8,9]).

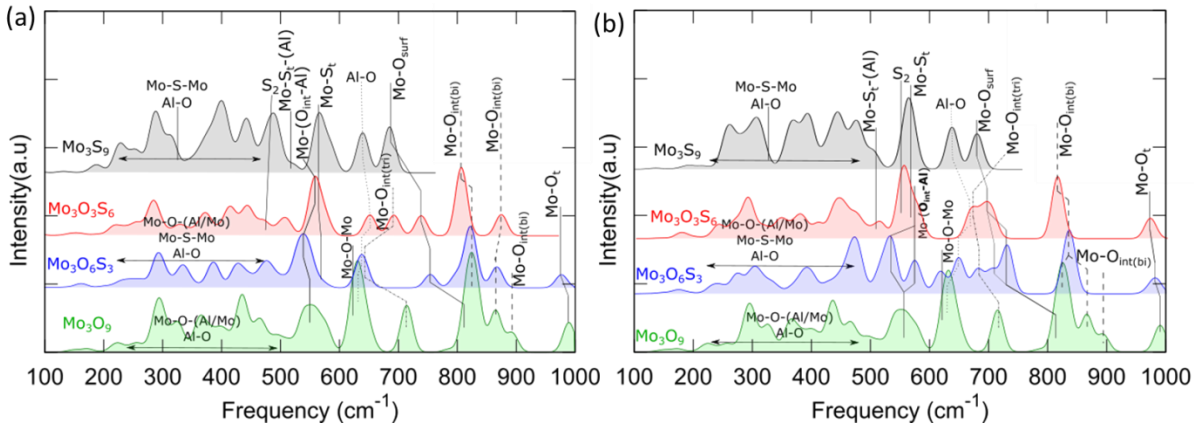

Figure S10. Simulated IR-spectrum for relevant intermediates during oxide to trisulfides transformation: a) Path-1 and b) Path-2.

The simulated IR spectrum of various Mo-oxides, oxysulfides, and trisulfides for Path-1 (a) and Path-2 (b) using a DFPT approach allows monitoring all the fundamental frequency modes of the oxysulfides clusters and their evolution during sulfidation. The contribution of alumina has been kept limited to the atoms located in the closest interacting region around the cluster (all other bulk atoms are being frozen).

The modes concerned with alumina are present almost everywhere underneath. We see an apparent change in the simulated IR spectra going from oxide to trisulfide. As discussed for EXAFS, the disappearance of Mo-O_t peak occur at a later sulfidation degree for path-2. The

evolution towards lower frequency is even true for Mo-O_{int} and Mo-O_{surf} and indicates the weakening of the interaction between oxysulfides and alumina. Mo-O_{int}-Al also disappears as more and more S are being replaced, and Mo-S-Mo (below 430 cm^{-1}) and S_2-dimer (540 cm^{-1}) peaks come into existence. The spectroscopic analysis clearly shows structural changes during the transformation; though, the alumina modes underneath complicate this analysis somewhat.

5.3. Vacancy creation on supported Mo_3O_9

Creating the O-vacancy from Chain-Mo_3O_9 is significantly endothermic. The ΔE of the following (Mo_3O_9 + H_2 → Mo_3O_8 + H_2O) reaction may vary from 0.2 eV to 1.76 eV depending on the type of oxygen is being removed. Creating the vacancy site by removing the terminal oxygen is exceptionally high (at least 1.14 eV). However, removing the bridging and some of the interfacial oxygens are comparatively easy. The empty octahedral site is highly unfavorable but creating a tetrahedral site at the edge is less endothermic than octahedral vacancy. Further removal of oxygen is even more expensive than the first one and could vary from 0.51- 1.89 eV based on the removing oxygen type.

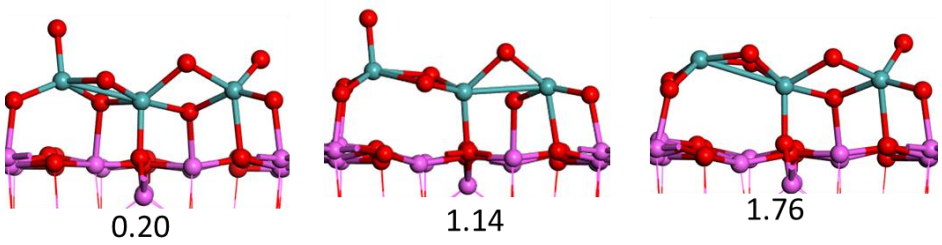

Figure S11. Mo_3O_8 structures after creating vacancy using H_2 and respective reaction energy.

5.4. Thermochemistry of sulfidation of supported Mo_3O_9

Figure S12 Illustrates the thermodynamically possible most favorable O/S exchange path, and below, we have shown the O/S exchange for cyclic trimer. As we have observed for chain trimer, in a similar fashion, the terminal and bridging oxygen are first and easily replaceable

compared to the interfacial ones, even for cyclic trimer. A slight reconstruction is required to reach the most stable conformer of $Mo_3O_4S_5$, which costs about 0.5 eV (see Figure S12). The final structure is very similar to the triangular model of a-Mo_3S_9. Their thermodynamic comparison with other chain structures has been illustrated in Figure S12.

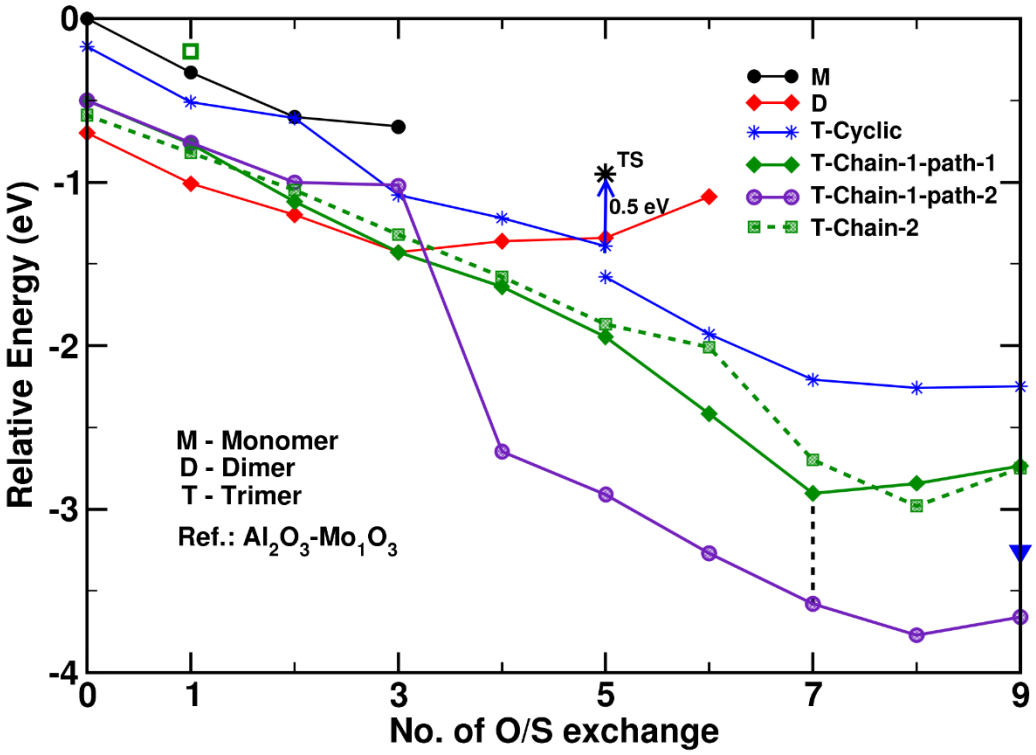

Figure S12. Thermodynamic energy (at 0K) diagram of various Mo-oxide models. Monomer adsorbed on alumina has been taken as a reference. The cyclic structure shows a transition at $Mo_3O_4S_5$ with respective transition state (TS) for transformation to a more stable conformer. Blue triangle represents the most stable triangular-Mo_3S_9 conformer on support. Unfilled green square represents the energy of exchanging O_{int} instead off O_t/O_{br}. Chain 1 corresponds to the starting oxide conformer represented in Figure S6a and chain 2, to the one of Figure S6b.

Thermodynamic energy comparison for various sizes of $MoO_3 \rightarrow MoS_3$ raises some crucial points, such as every O/S exchange is thermodynamically favorable except for some interfacial oxygen. Interestingly, the cyclic trimer is far less stable than the cyclic chain for sulfides, almost 1.5 eV. This is particularly important, as, in its gas phase, the triangular is more stable by about 1 eV than the chain of Mo_3S_9. By these observations, it appears that the Mo3 size will mainly exist in chain form. For the larger size, the chains are also more stable in the gas phase. Therefore, they might be more stable on support too. However, the formations of such chains without deformation can be questioned and needs further examination.

Chain-2 (Figure S8 e) and cyclic (Figure S8 a) conformers follow the general trend of O/S exchange: the bridging and terminal oxo-sites are being replaced first, followed by $O_{int(bi)}$ and $O_{int(tri)}$. The possibility of a similar effect of $O_{int(bi)}$ being replaced first and leading to the formation of S_2-dimer providing additional stability also exists for chain-2 and cyclic conformers. The appearance of the S_2-dimer increases the stability of chain-2 and cyclic by 0.44 eV and 0.46 eV from their non-dimer states, respectively.

By following the O/S exchange path, the final cyclic Mo_3S_9 structure is less stable than the chain-1-path-2 and chain-1-path-1 structure. Actually, we also found another triangular trisulfide conformer that exhibits an intermediate level of stability between chain-1-path-2 and chain-1-path-1. We will come back to this point later in the discussion on structural reconstruction aspects.

5.5. Kinetics of the sulfidation of supported Mo_3O_9

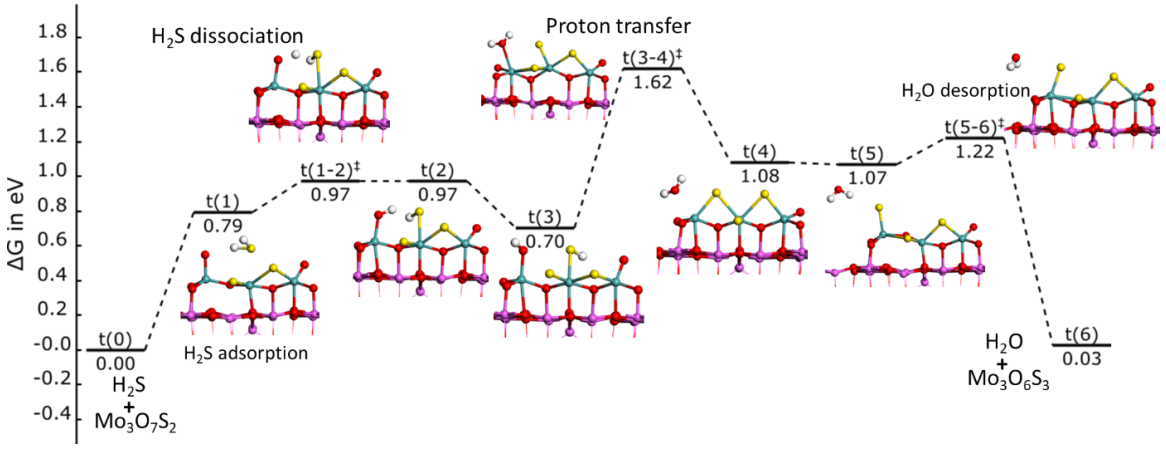

Figure S13. Free energy profile of O/S exchange involving terminal oxygen and H_2S. Color legend: red balls: O, blue balls: Mo, pink balls: Al, yellow balls: S, and white balls: H.

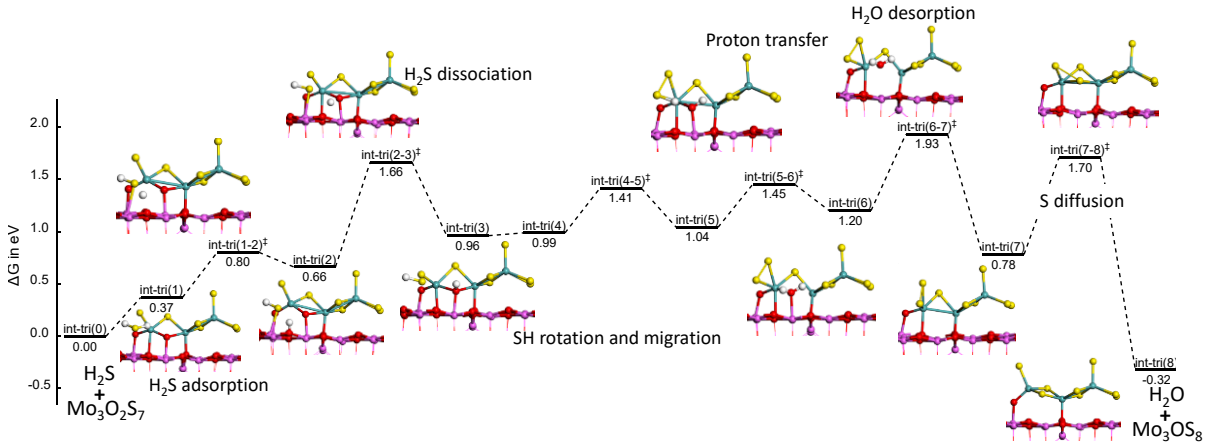

Figure S14. Free energy profile of O/S exchange involving interfacial-tridentate oxygen using H_2S. Color legend: red balls: O, blue balls: Mo, pink balls: Al, yellow balls: S, and white balls: H.

The strength of H_2S adsorption on alumina may vary depending on the adsorption site and the orientation of H_2S. For example, H_2S adsorption energy (on support) for $O_{int(bi)}$ and $O_{int(tri)}$ differs by 0.18 eV (at 0 K). In both cases, H_2S is adsorbed on an octahedral site of Al but differs by a 45° rotation. Different hydrogen bonding through the oxygen of support (2.72 Å

vs. 3.36 Å) and direct access to the octahedral Al site for H_2S adsorption (2.58 Å vs. 2.76 Å) contribute to the additional stability.

5.6. Electronic energy profiles for chain-Mo_3O_9 sulfidation by O/S exchange

a) bridging

b) terminal

c) Interfacial -bidentate

d) Interfacial -tridentate

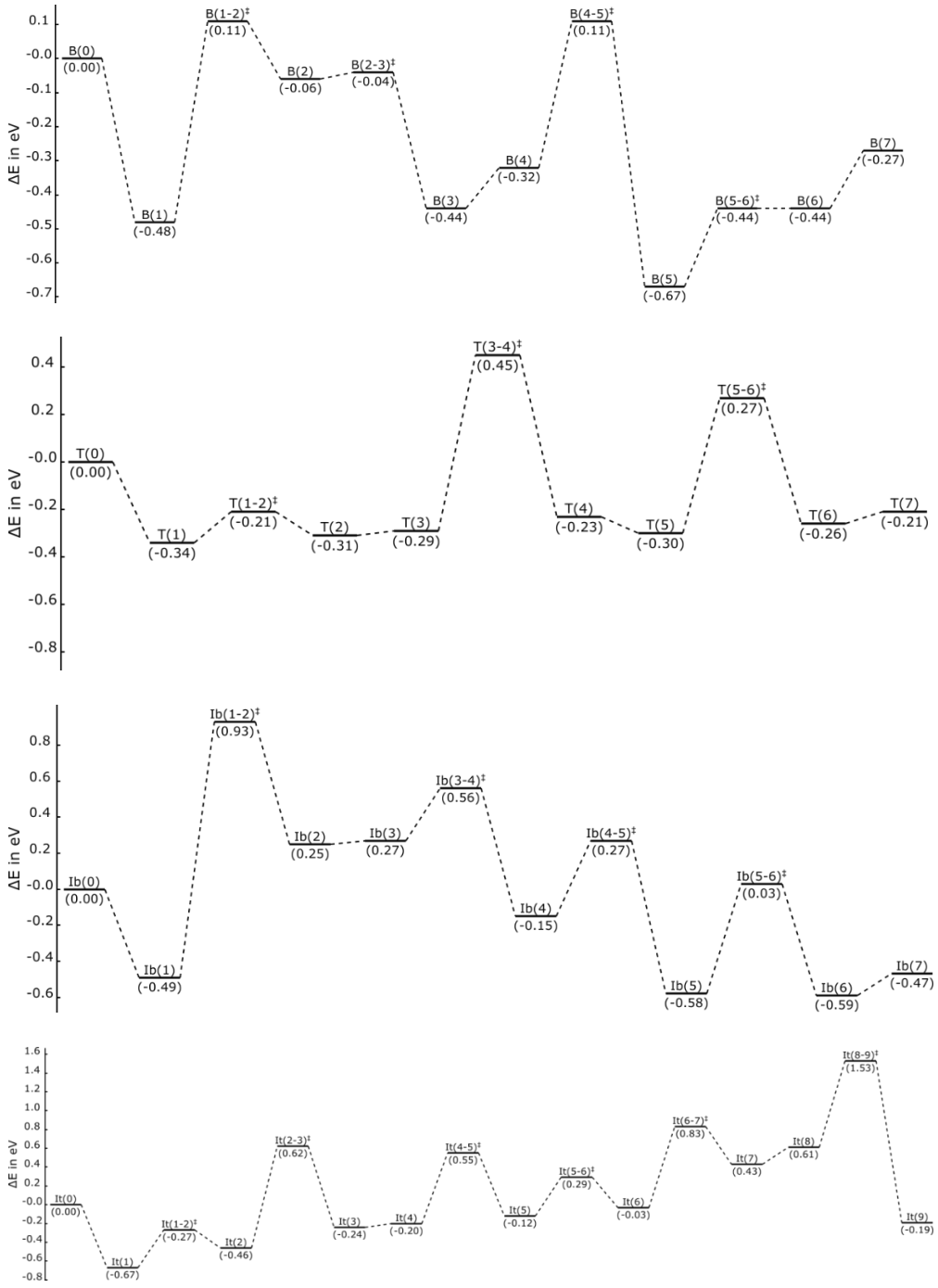

Figure S15. Electronic energy profile of O/S exchange by H_2S/H_2O: a) bridging, b) terminal, c) interfacial bidentate, and d) interfacial tridentate.

Considering these energetic profiles and analyzing the effect of entropy and thermal corrections, we notice that these corrections increase the barriers by about +0.6 eV to +0.8 eV for bridging and terminal oxygen, albeit the rate-limiting step remains unchanged. However, the barriers for $O_{int(bi)}$ and $O_{int(tri)}$ are increased by only +0.4 eV. This entropy effect is found to be directly proportional to the adsorption energy of H_2S either on the Mo cluster or on the support. The weakest H_2S adsorption is for terminal oxygen (-0.34 eV) due to weak hydrogen bonding through present O/S on the cluster and acquires the highest entropy effect +0.79 eV that leads to the more considerable enhancement in the activation energy difference of the terminal and bridging oxygen. Likewise, $O_{int\text{-}tri}$ has the most substantial adsorption (-0.67 eV) and obtain the weakest destabilization (+0.37 eV) due to entropy and thermal contributions. Consequently, including entropy and thermal contributions reveal that the activation free energies for O/S exchange between terminal oxo-species and interfacial O-species are less pronounced than without these corrections. The difference in activation energy of terminal and interfacial reduces to 0.2 eV, making even the terminal oxygens kinetically difficult to exchange while the bridging species are kinetically favored. Therefore, including entropic effects is required to understand better why terminal oxo-species are present in $Mo_3O_3S_6$ as observed by EXAFS.[6,8]

6. Sulfidation of supported cyclic Mo_3O_9

a) terminal

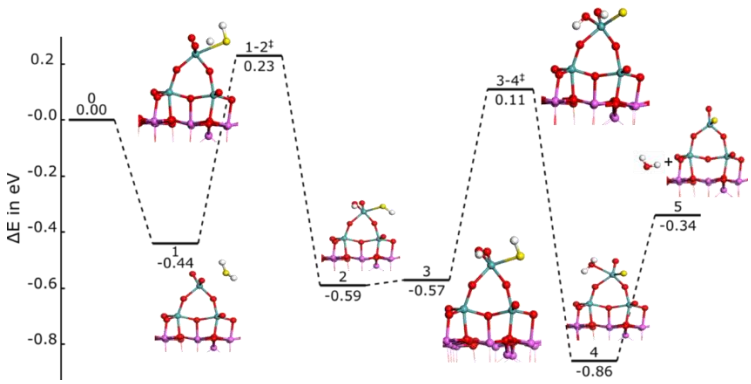

b) bridging

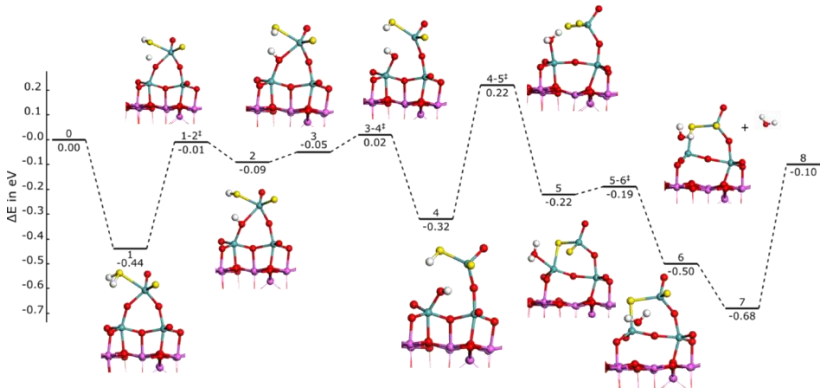

c) interfacial-bidentate

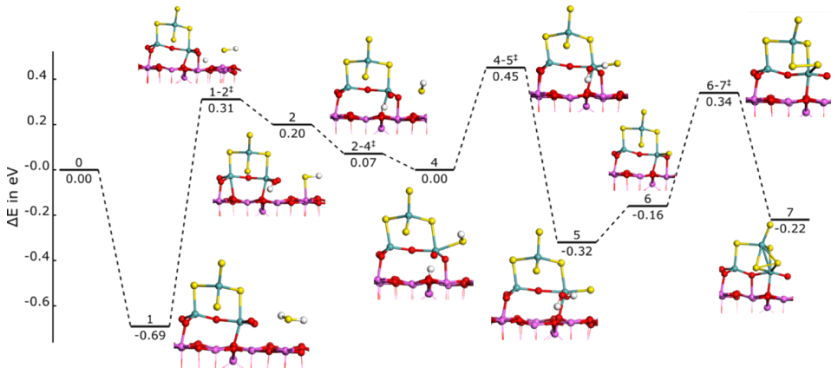

d) interfacial-tridentate

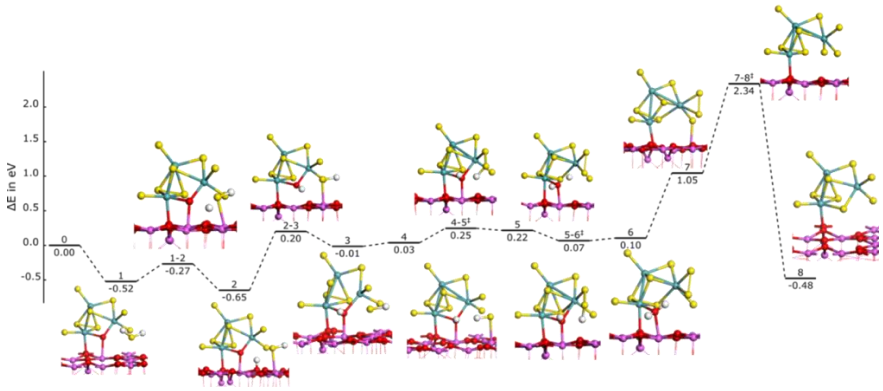

Figure S16. Mo-Oxides to Mo-sulfides transformation by O/S exchange (Cyclic-Mo_3O_9 → TR-Mo_3S_9) supported on alumina: a) cyclic-trimer, b) chain-1 path-1, c) chain-1 path-2 d) chain-1-combined, e) chain-2.

Terminal Oxygen: Starting from H_2S adsorption on the clusters followed by H_2S dissociation that involves the proton transfers to the oxygen and leads to the formation of SH, OH. The activation energy is similar to that of terminal oxygen in the chain (+0.67 eV). Some SH and

OH rotations are required to get the appropriate intermediate for second proton transfer, leading to water formation. The final step is the desorption of water.

Bridging Oxygen: Thermodynamically, the second oxygen replacement occurs at the bridging site. During kinetics, similar steps are followed. The second proton transfer is the rate-limiting step and requires about 0.66 eV activation energy. The Bridging and terminal oxygen have similar kinetic limitations; therefore, they could be replaced simultaneously for the cyclic trimer.

Interfacial bidentate: As in the case of chain IB replacement, the adsorption of H_2S takes place on support. Dissociation of H_2S requires about 1 eV, and the rate-limiting step is the second proton transfer. The energy needed for activation is about 1.14 eV, which is significantly lower than the energy of the interfacial bidentate chain, approximately 1.42 eV. The desorption is relatively easy as the water remains on the cluster and does not move to the surface for the interfacial bidentate chain. Finally, a slight reconstruction of am oxysulfide cluster leads to a stabler conformer.

Interfacial tridentate: These are the most challenging oxygen to be replaced. The activation of H_2S takes place on the surface. The earlier steps are not as expensive as water desorption and sulfur diffusion. This is similar to the case of the interfacial tridentate chain. The water desorption step is the second most costly step after sulfur diffusion. Water desorption requires 1.7 eV and reconstruction >2.5 eV, though entropy correction could change the order as in the interfacial tridentate chain.

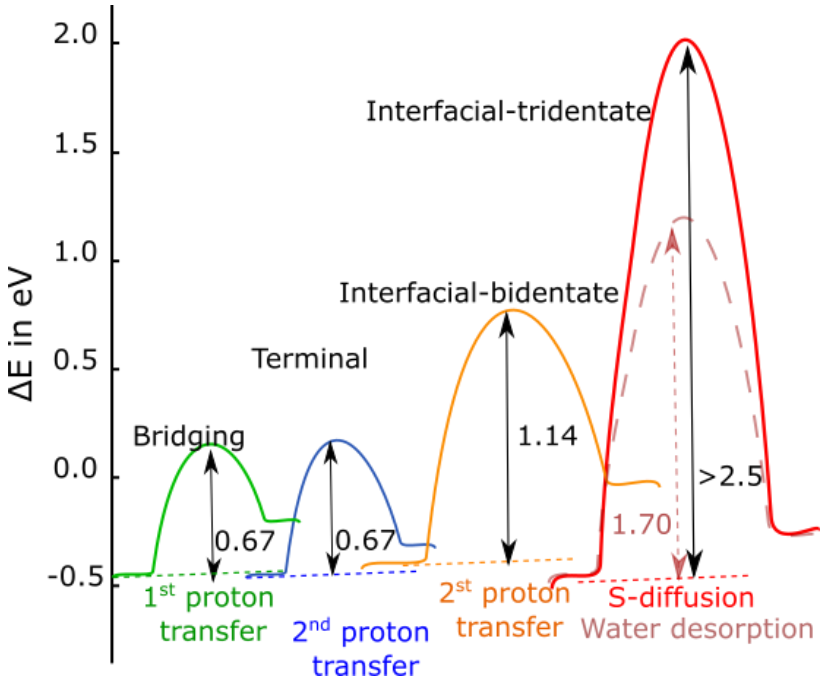

Figure S17. Energetics span analysis of O/S exchange for various types of oxygen present in cyclic trimer at 0K.

The energetic span analysis has been represented in **Figure S17** with the respective rate-determining step. The O/S replacement trend remains similar between chain and triangular. Bridging is the most easily replaced, followed by the terminal. Interfacial bidentate and tridentate remain the most difficult to replace. The RDTS for a similar class of oxygens is also the same.

7. Thermodynamics and kinetics of O or S removal

7.1. Thermodynamic energy plot O/S removal

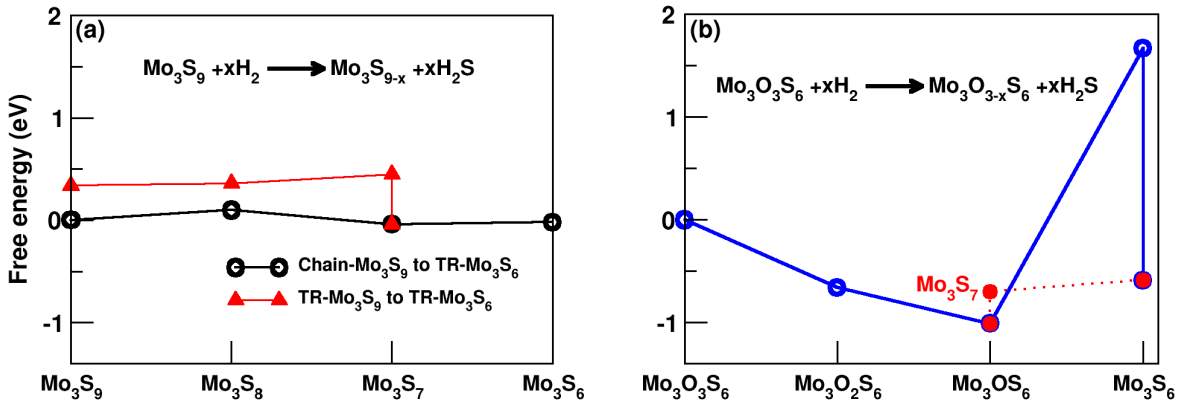

Figure S18. Thermodynamic energy plot for a) trisulfide to disulfide transformation and b) oxysulfide to disulfide reduction by H_2.

7.2. Sulfur removal from Mo_3S_9 to Mo_3S_6

a) Terminal-S_2

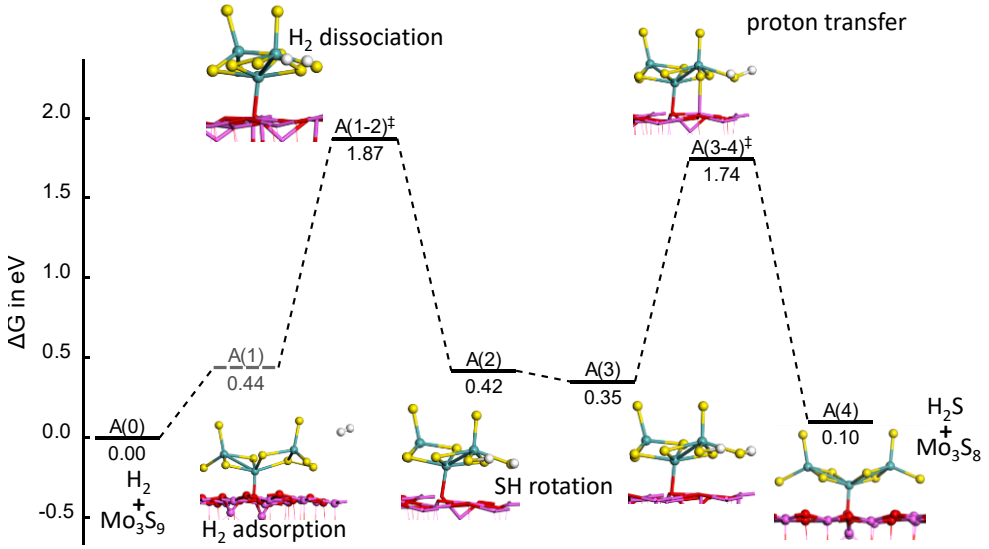

b) Bridging-S

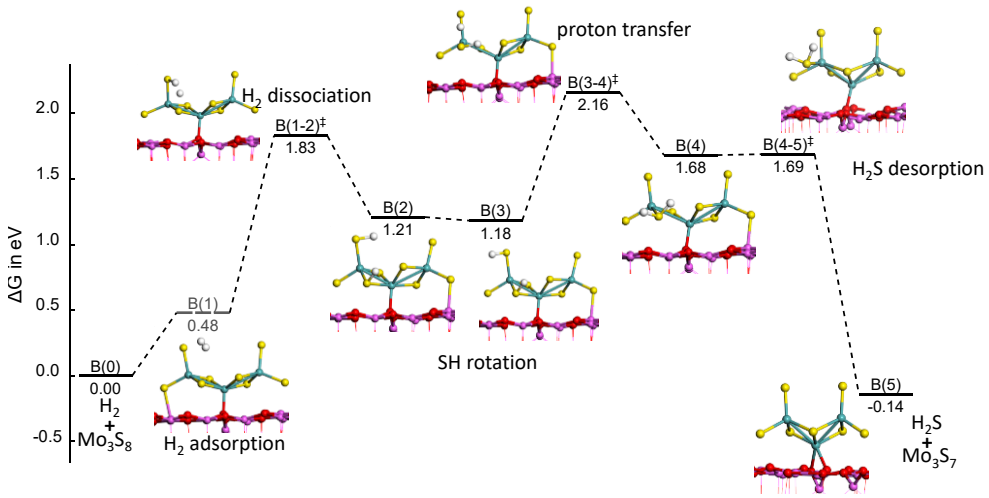

Figure S19. Free energy profile for removing S by using H_2 : a) Terminal-S_2 and b) bridging-S. A(1) and B(1) corresponding to H_2 physisorbed precursor states are subject to higher uncertainties on their entropic contribution so their free energy level are represented with a dashed lines. Color legend: red balls: O, blue balls: Mo, pink balls: Al, yellow balls: S, and white balls: H.

a) Terminal-S_2

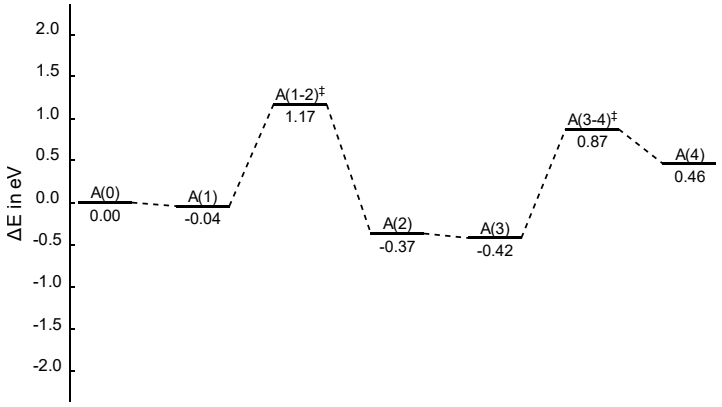

b) Bridging-S

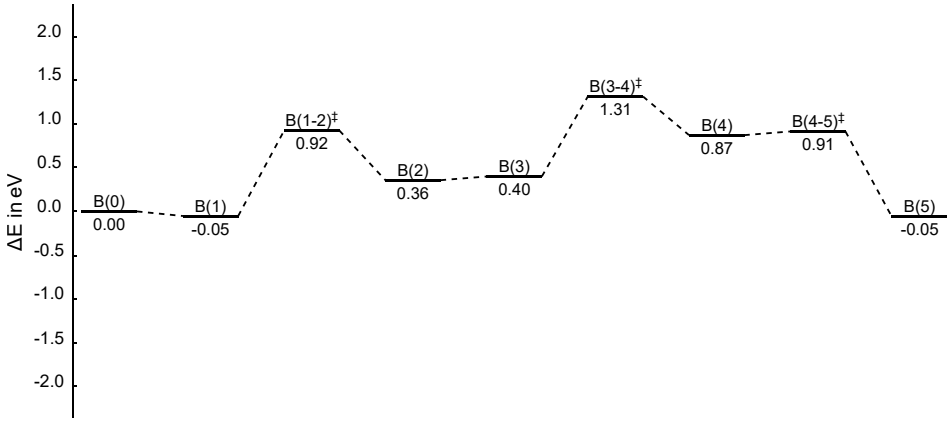

c) Terminal-S

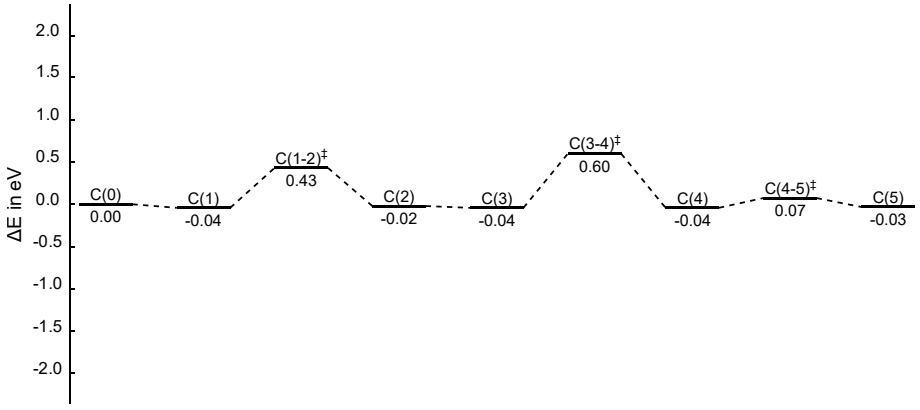

Figure S20. Electronic energy profiles of Mo-trisulfide to Mo-disulfide transformation by removing the S on supported alumina: a) terminal-S_2, b) bridging-S, c) terminal-S.

7.3. Oxygen removal with H_2 from $Mo_3O_3S_9$ to Mo_3S_6

a) interfacial-bidentate

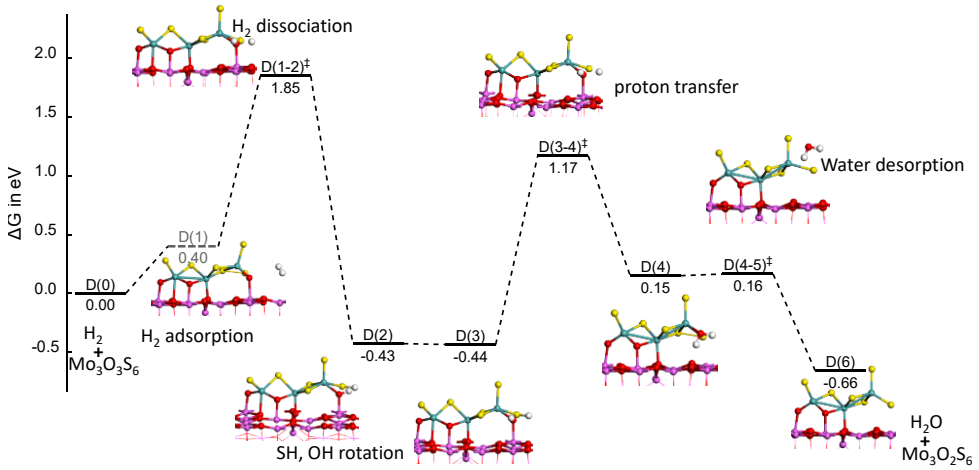

b) interfacial-tridentate

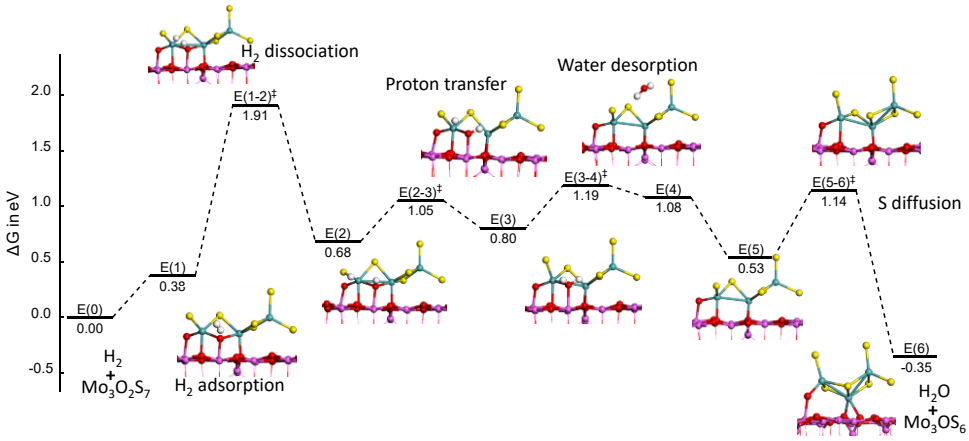

c) interfacial-bidentate O/S exchange

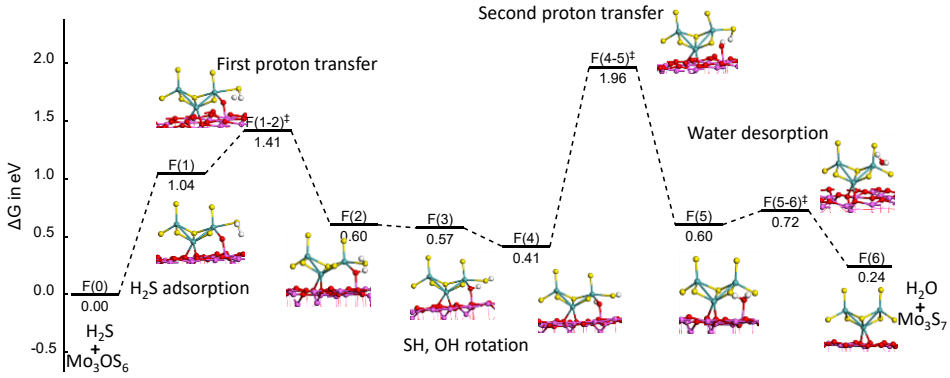

Figure S21. Free energy profile for oxygen removal using H_2 a) interfacial bidentate b) interfacial tridentate c) O/S exchange using H_2S/H_2O, $Mo_3OS_6 \rightarrow Mo_3S_7$.

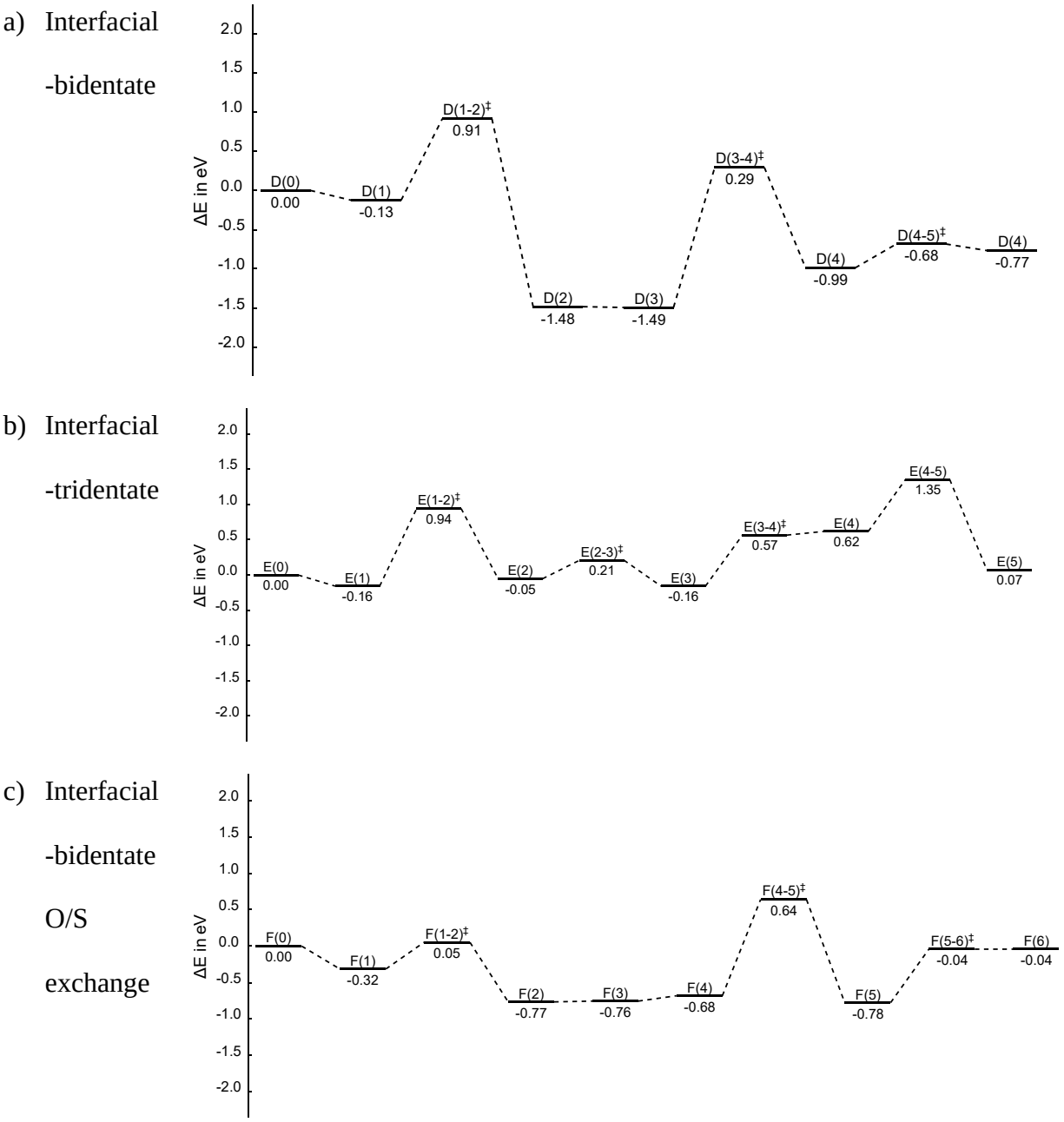

Figure S22. Electronic energy profiles of oxysulfides to disulfide reduction by removing the O on supported alumina: a) interfacial bidentate, b)interfacial tridentate, and c) interfacial bidentate O/S replacement.

The activation free energies for H_2 dissociations are relatively high $\left(\Delta G^{\ddagger}{}_{D_{0\to 2}} = 1.85 \text{ eV}\right)$ and leads to the formation of one SH and one OH group (**Figure S21**a). These values are similar to the activation for H_2 dissociation on Mo_3S_9 ($\Delta G^{\ddagger}{}_{A_{0\to 2}} = +1.87$ eV). This H_2 dissociation is

followed by SH and OH rotations and proton transfer from SH to OH to produce H_2O. Interestingly, the water desorption is kinetically easier than in the case of O/S exchange ($\Delta G^{\ddagger}_{D_{4\to5}} = +0.16$ eV and $\Delta G^{\ddagger}_{int-tri_{6\to7}} = +0.73$ eV) However, in O/S exchange, the S diffusion and water desorption are concerted, explaining the excessive energy cost for water desorption. In the $Mo_3O_2S_6$→Mo_3OS_6 transformation, after the removal of the water, a slight rearrangement with modest activation energy ($\Delta G^{\ddagger}_{E_{5\to6}} = +0.61$ eV) leads to a triangular kind of Mo_3OS_6 entity as in the case of $Mo_3S_8 \rightarrow Mo_3S_7$.

Considering the last reduction step, $Mo_3OS_6 \rightarrow Mo_3S_6$, we found that the process is thermodynamically unfavorable (+2.68 eV) because it goes through a high-energy Mo_3S_6 intermediate which must then reconstruct into the most stable triangular Mo_3S_6. Since removing the final oxygen seems to be a difficult step, we propose to come back to an O/S exchange process as already studied for the previous steps to overcome this issue. Similarly, the elementary steps combine H_2S adsorption, dissociation of H_2S, and formation of SH, OH groups, SH-OH reorientation, proton transfer that leads to water formation. The TS of the proton transfer exhibits the highest free energy level ($\Delta G^{\ddagger}_{F_{0\to5}} = +1.96$ eV). Once Mo_3S_7 is formed, it will follow the S removal path already studied before (Mo_3S_7→ Mo_3S_6).

8. Mo_3S_9 reconstruction followed by S-removal

8.1. Chain to triangle reconstruction of Mo_3S_9

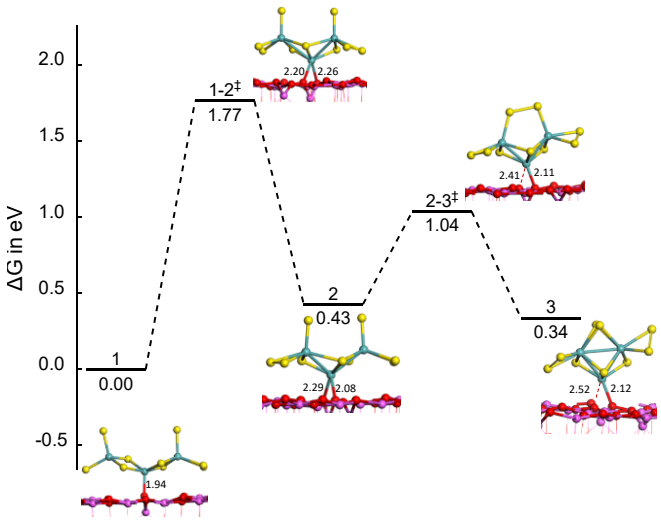

Figure S23. Free energy profile of Chain-Mo_3S_9 to TR-Mo_3S_9 transformation (ΔG = $G_{product} - G_{chain\text{-}Mo3S9}$).

Diffusing the S from its bridging site to the terminal site enables the formation of a terminal dimer. The first step involves the breaking of one Mo-S bond of a μ_2-S to form a μ_1-S_2, and the simultaneous formation of a new Mo-S bond from another μ_2-S converted into μ_3-S. This step requires a significant free energy cost of $\Delta G^{\ddagger}_{1\rightarrow 2}$ = 1.77 eV. It must be underlined that the corresponding TS is stabilized by shifting the position of the Mo central atom on the alumina. This Mo atom becomes in a bridging position between two oxygen atoms of alumina, whereas it was located on top of one oxygen before with a short Mo-O bond length (1.94 Å). This bridging position is rather symmetric at TS (Mo-O=2.20 and 2.26 Å). In the second step, the closing of the triangular occurs with the formation of a μ_2-S_2 bridging two Mo atoms at a moderate activation energy. The third Mo atom moves back to a nearly top position on O of alumina (Mo-O=2.12 and 2.52 Å, for the final product).

8.2. Triangular-Mo_3S_9 to triangular-Mo_3S_6 transformation

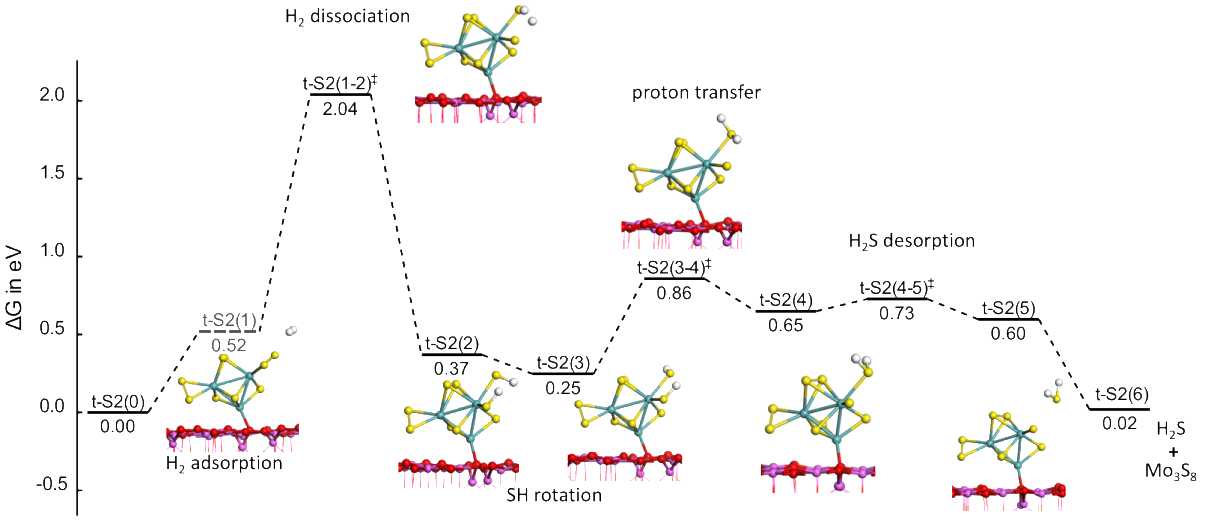

Figure S24. Free energy profile of S removal from terminal-S_2 of Mo_3S_9.

9. Interaction and diffusion of sulfides

9.1. Strength of interaction of various species with alumina support

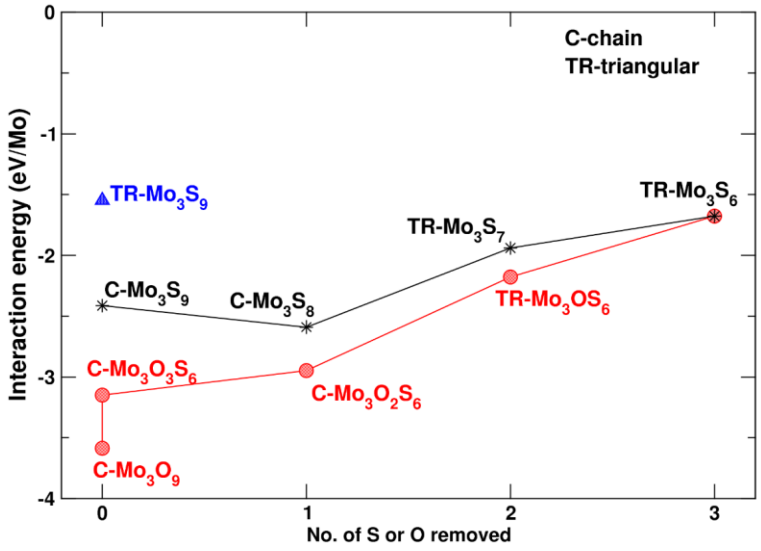

Figure S25. Interaction energy of Mo-oxide, -oxysulfides, -sulfides, and intermediates with the alumina (100) surface as a function of S or O removals normalized by per Mo. (interaction energy $= E_{*clusters} - E_{*} - E_{cluster}$; * is surface).

The mobility (diffusion) of intermediates are key steps for determining which intermediate might be the most prone to grow on the alumina surface. For that, the interaction energy descriptor reported in (**Figure S25**) for some suitable oxide, oxysulfide, trisulfide, and disulfide species provides a first estimation of the strength to guide us towards the species for which the diffusion is essential. The stronger interaction of Mo oxides with alumina support through Al-O-Mo linkage is coherent with chemical intuition.[10] The interaction energy systematically decreases with increasing the number of sulfur atoms replacing oxygen atoms. The interaction could be weaker for Mo sulfides due to the weaker number of Al-S(O)-Mo linkages as reported for MoS_2.[11] Hence, the mobility of oxide precursors and oxysulfide intermediates is suspected to be significantly prevented due to strong interaction through Mo-O-Al linkage compared to sulfides, where only one Mo-O-Al bridge exists. Moreover, the nature of the conformer also influences the interaction energy (**Figure S25**): all chain-like

clusters (including Mo_3S_9) are more strongly bonded to alumina than triangular (or cyclic) ones. The weaker interaction of triangular-Mo_3S_9 and Mo_3S_6 implies that they would be the more mobile species diffusing on the surface and allowing the formation of larger MoS_3 or MoS_2 clusters.

9.2. Diffusion path

To understand the interaction of various sites of support with MoS_3 or MoS_2 clusters, we have investigated some relevant cases of diffusion. We assumed the cluster would move on the surface translationally by mapping two directions of the surface plane (**Figures S26-S29**). We have not investigated the rotation of the cluster on the surface. The barrier shown in the main text is the lowest barrier required for the cluster to reach its original site from both directions (including the zero-point energy and frequency corrections). From interaction energy, we already know the interaction of TR-Mo_3S_9 is significantly weaker than chain-Mo_3S_9 but similar to Mo_3S_6. We also suspect a similar trend for the diffusion path as we restrict the diffusion to only translational mode.

Chain-Mo_3S_9 shows the highest barrier along the horizontal and vertical axes in contrast with triangular-Mo_3S_9 and Mo_3S_6. Chain-Mo_3S_9 possesses a stronger interaction with support only with one single Mo-O_{surf} bond. However, triangular-Mo_3S_9 and chain-Mo_3S_6 interact with support weakly and involve two Mo-O_{surf} bonds. During diffusion, chain-Mo_3S_9 breaks only Mo-O_{surf} bond, but triangular-Mo_3S_9 and Mo_3S_6 break only one Mo-O_{surf} band and remain attached with support with another one. In all cases, chain-Mo_3S_9, triangular-Mo_3S_9, and Mo_3S_6, the largest activation energy was observed for the transition states and intermediates those passe through Al^{IV} in proximity. The presence of Al^{IV} in the neighborhood seems to destabilize the transition states (see TS 2-3‡ and 4-5‡ in figure S26, S27, S28). However, the

intermediates are only destabilized for chain-Mo_3S_9 (intermediate 2,3 and 5 for figure S26) but not triangular-Mo_3S_9 or Mo_3S_6. This is mainly due to coordination from support, as chain-Mo_3S_9 has only one anchoring site compared to triangular species, which are stabilized by the other site when the Al^{IV} site is nearby.

Furthermore, as a result, the triangular species are slightly tilted in the reverse direction with respect to their previous intermediate (see 2 and 3 in Figure S27, S28). No Mo-Al interaction was observed in any case. The same is even true for monomeric species (Mo_1S_3). The most stable site is the hollow site. The intrinsic activation barrier is lowest for the triangular-Mo_3S_9 followed by Mo_3S_6 and chain-Mo_3S_9. This observation is consistent with the interaction energy of individual species.

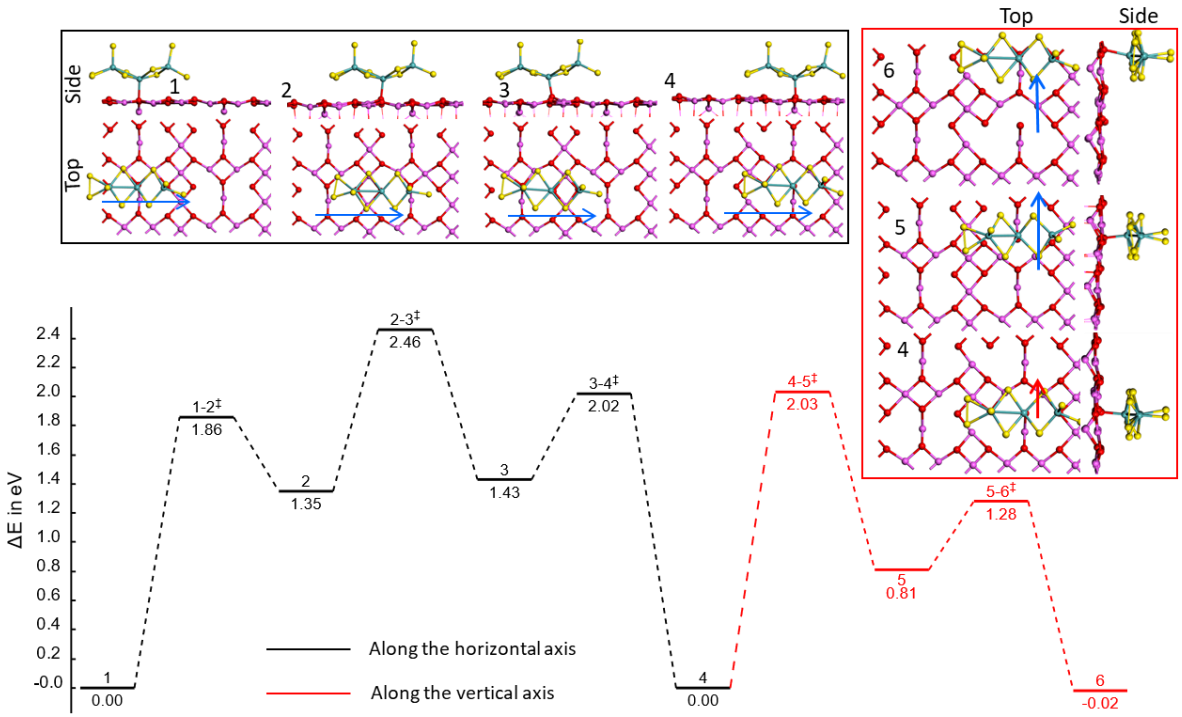

Figure S 26: Electronic energy profile for the diffusion of chain-Mo_3S_9 along the horizontal and vertical axis.

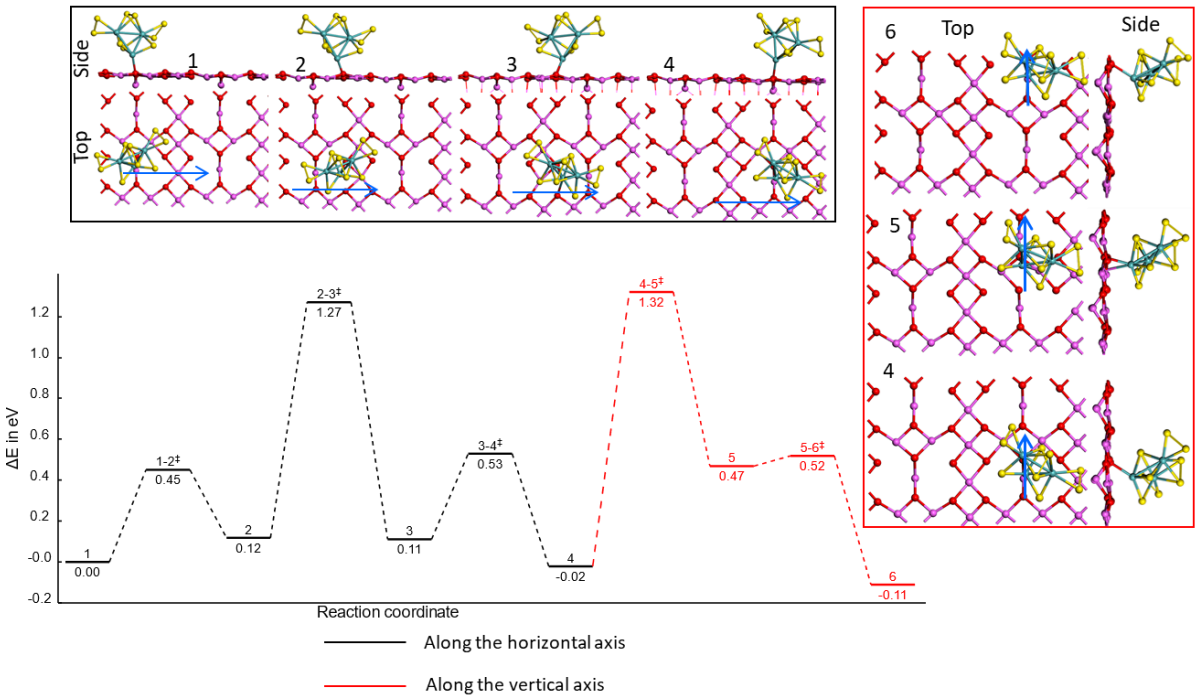

Figure S27. Electronic energy profile for the diffusion of TR-Mo_3S_9 along the horizontal and vertical axis.

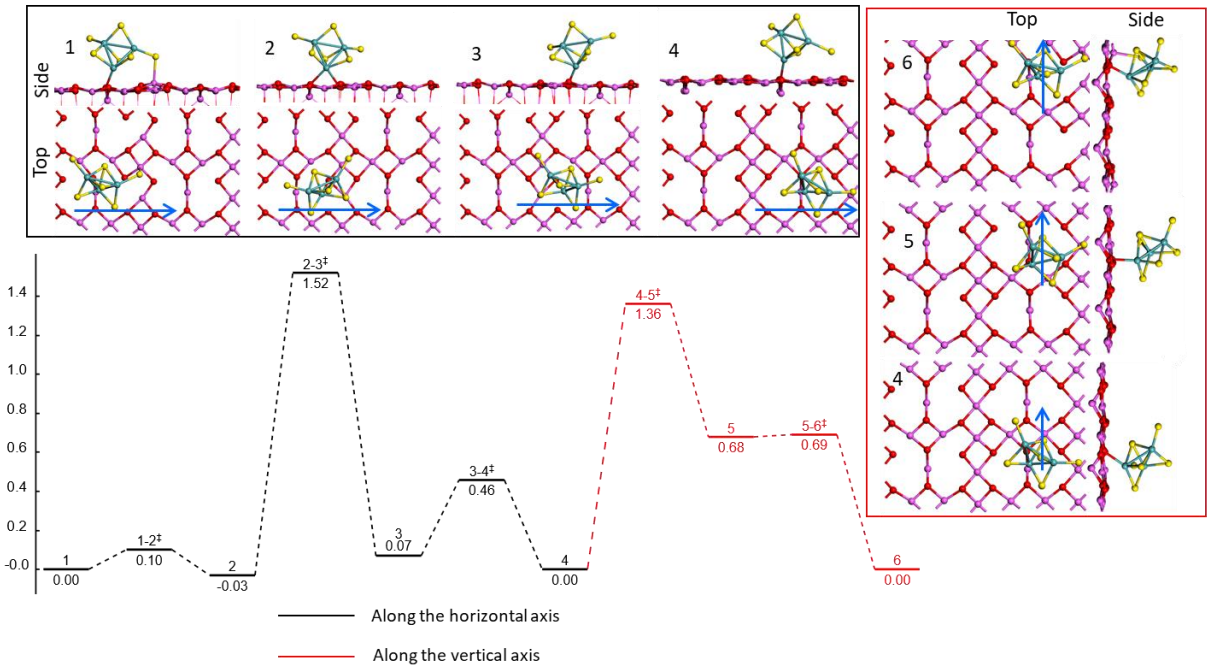

Figure S28. Electronic energy profile for the diffusion of Mo_3S_6 along the horizontal and vertical axis.

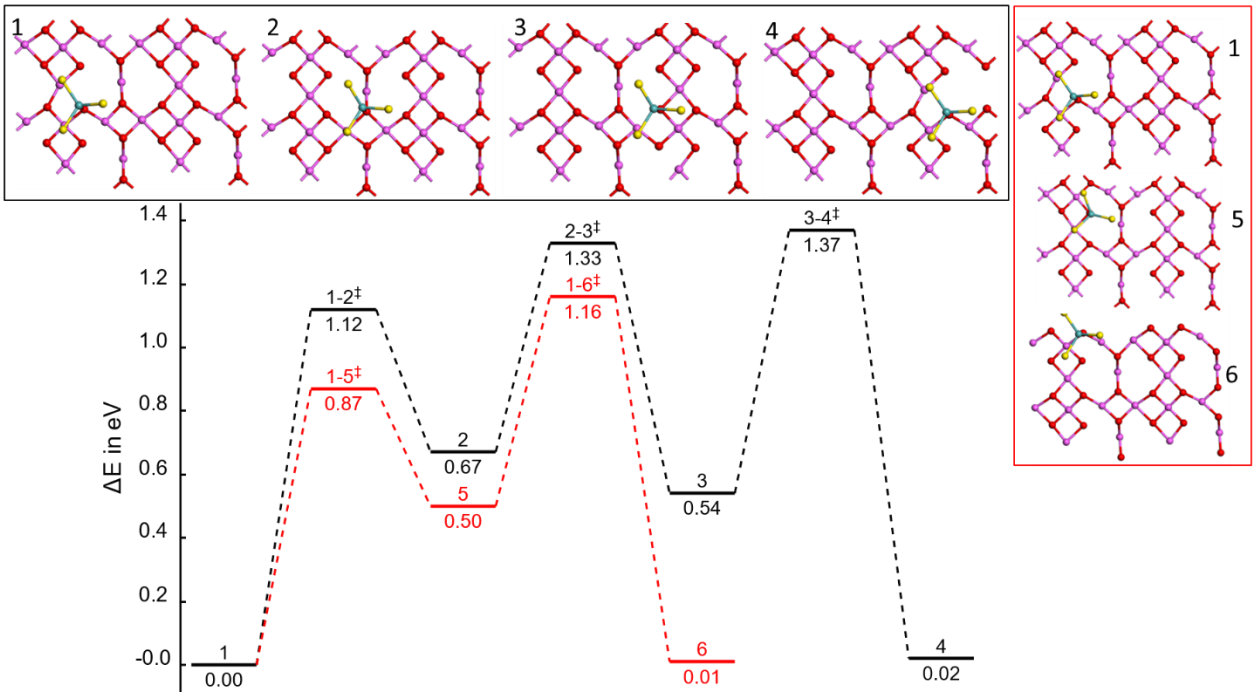

Figure S29. Electronic energy profile for the diffusion of Mo_1S_3 along the horizontal and vertical axis.

10. Complete free energy profile of Mo_3O_9 to Mo_3S_6

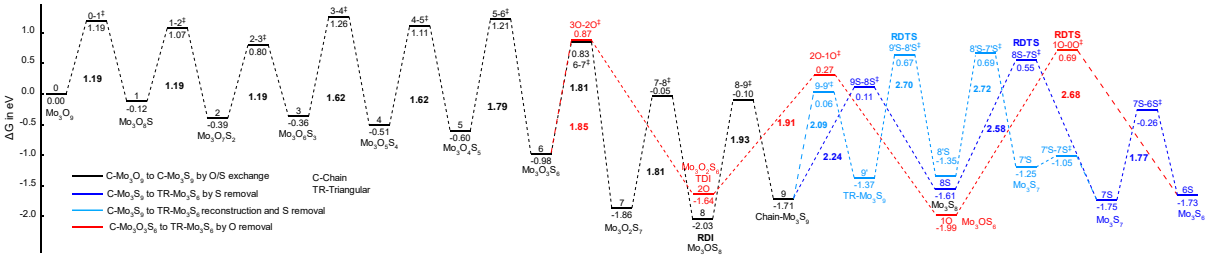

Figure S30. Entire reaction path from Mo-oxides to Mo-disulfides with all the respective intermediates and activation energies. Red: oxysulfide pathway, black: chain trisulfide pathway, and blue: triangular trisulfide pathway. Respective RDI and RDTS have also been mentioned.

11. Size effect on S/O exchanges and S removal

We provide some insights into the effect of cluster size on the kinetics of O/S exchange and S-removal for monomeric species (Mo_1O_3 or Mo_1S_3 and compare it with the trimer case (Figure 8 in the main text). The detailed stepwise mechanism and limiting steps are shown in (**Figure S7**). Interestingly, the kinetic limitation to replace interfacial oxygen remains also valid for monomers. Interfacial oxygen exchange costs 1.35 eV as compared to 1.14 eV for terminal oxygen. In both cases, the proton transfer remains the rate-limiting step. The comparison of the monomer and the trimer reveals that the O/S exchange for monomer is more advantageous than for trimer, and its activation free energy is by 0.58 eV lower, while thermodynamic aspects are equivalent. We suspect the greater coordination for small Mo_1O_3 entities compare to larger ones (Mo_3O_9); therefore, O/S exchange should be difficult, but we observe the reverse. This unexpected observation indicates that the sulfidation mechanism is faster with small size species such as Mo_1O_3. In particular, these small entities cannot explain the presence of residual non-sulfided Mo species as often observed experimentally.[6,8]

By contrast, the further S removal from Mo_1S_3 to Mo_1S_2 is found to be impossible kinetically (free activation energy of >2.7 eV), which is significantly than for Mo_3S_9 species (2.58 eV). At the same time, it is thus more beneficial to sulfide Mo_1O_3, and essentially impossible to transform into Mo_1S_2. However, more calculations are required to validate this point. This result may indicate that smaller trisulfides entities are less prone to change into disulfides than larger ones. This would imply that the growth towards larger $Mo_{3n}S_{9n}$ oligomers would enhance the S-removal step leading to $Mo_{3n}S_{6n}$ disulfides.

11.1. Kinetics of S removal from Mo_1S_3

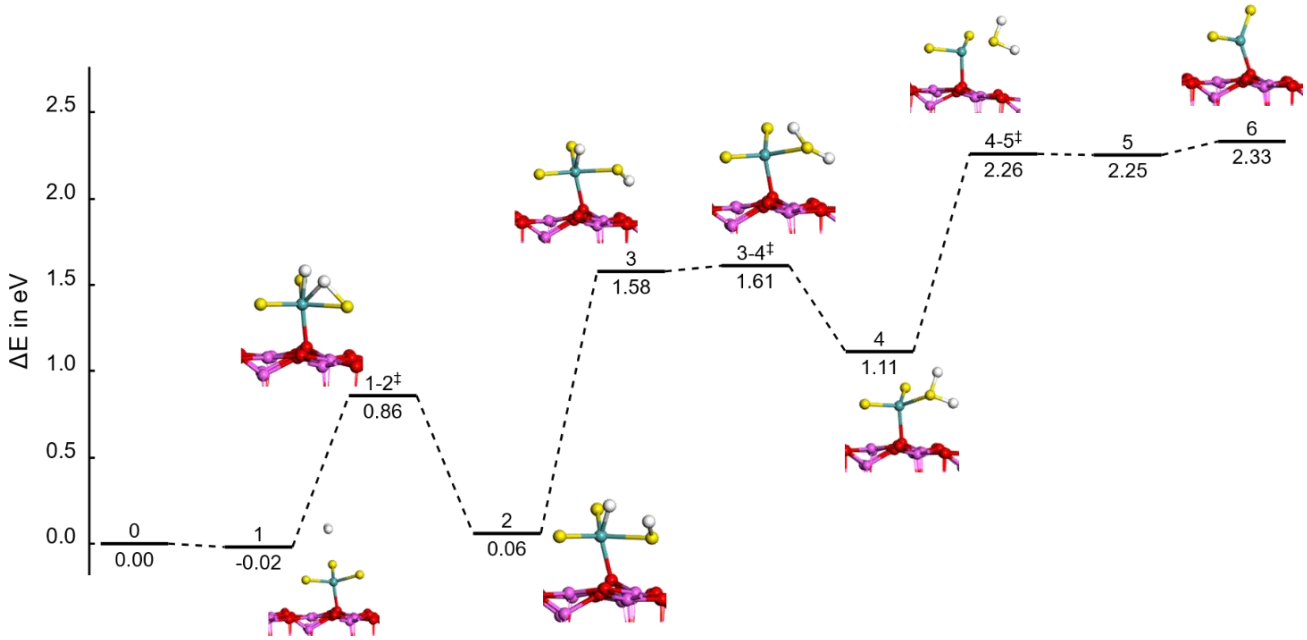

Figure S31. Free energy profile of S removal from Mo_1S_3.

Removing the sulfur atom from tiny trisulfide entities such as Mo_1S_3 is highly endothermic. The comparison in the main text has been made by calculation the ΔG for the respective limiting step.

11.2. Kinetics of S removal from Mo_6S_{18}

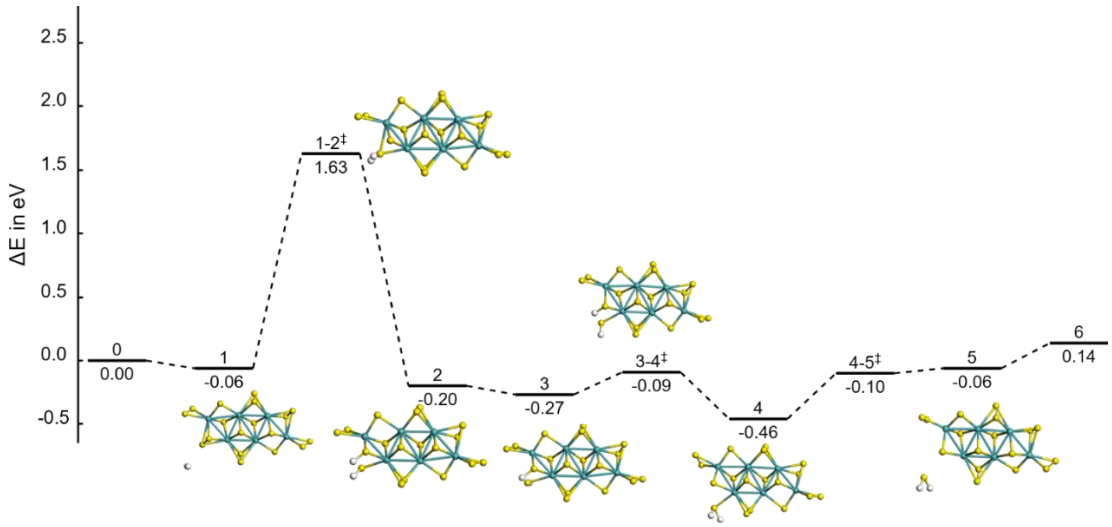

Figure S32. Free energy profile of S removal from bridging-S_2 of Mo_6S_{18}.

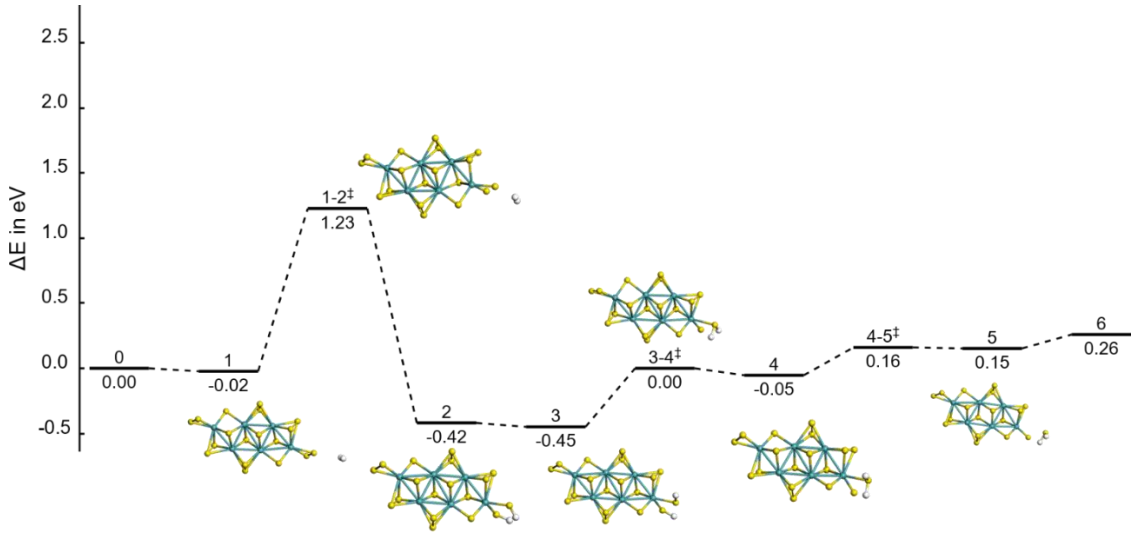

Figure S33. Free energy profile of S removal from terminal-S_2 of Mo_6S_{18}.

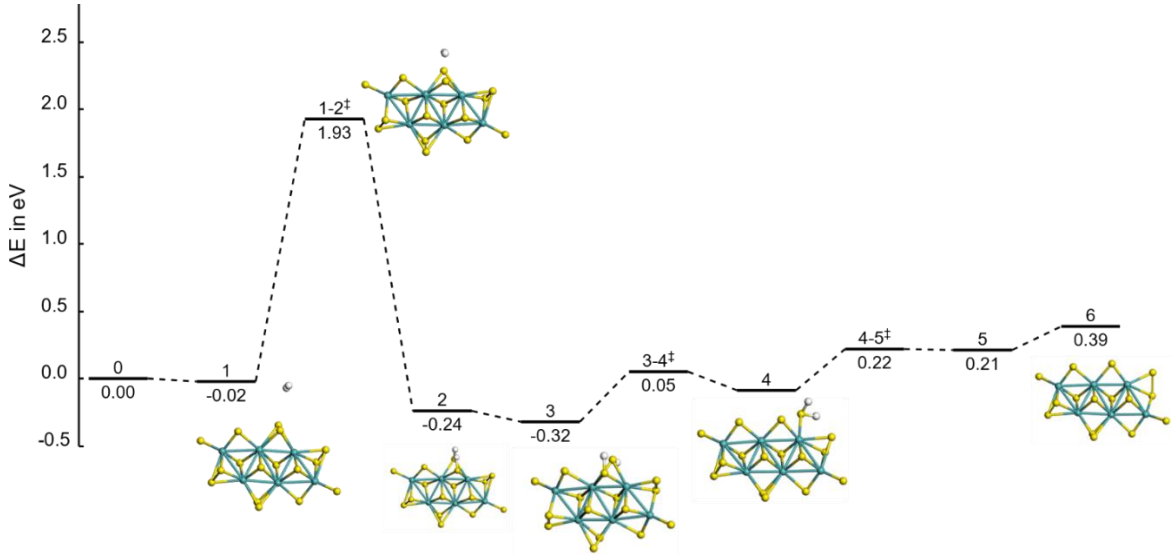

Figure S34. Free energy profile of S removal from bridging-S_2 of Mo_6S_{16}.

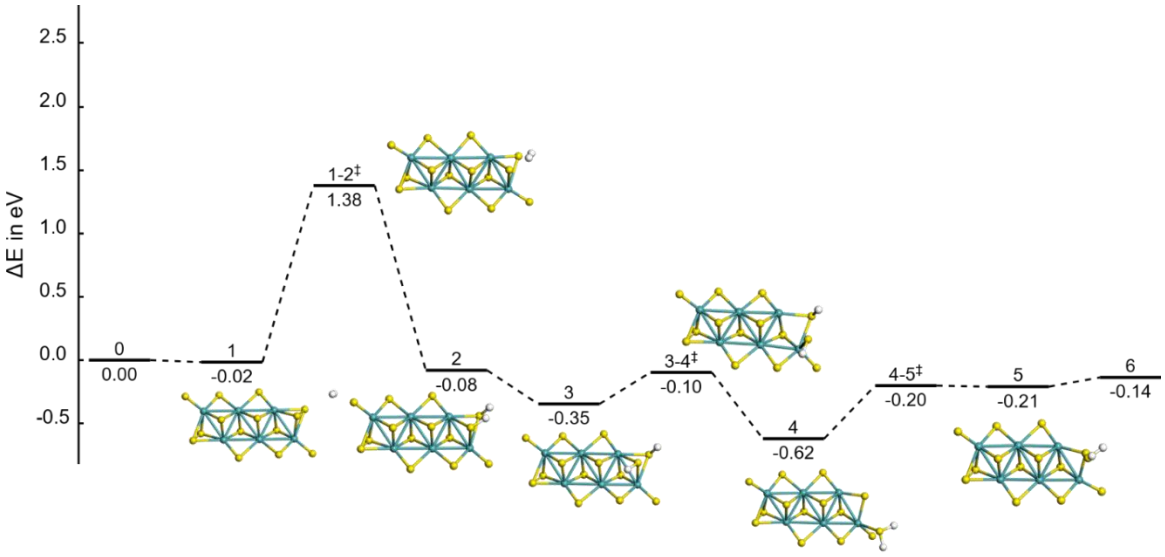

Figure S35. Free energy profile of S removal from bridging-S_2 of Mo_6S_{14}.

11.3. Kinetics of S removal from 1D-Mo_4S_{11}

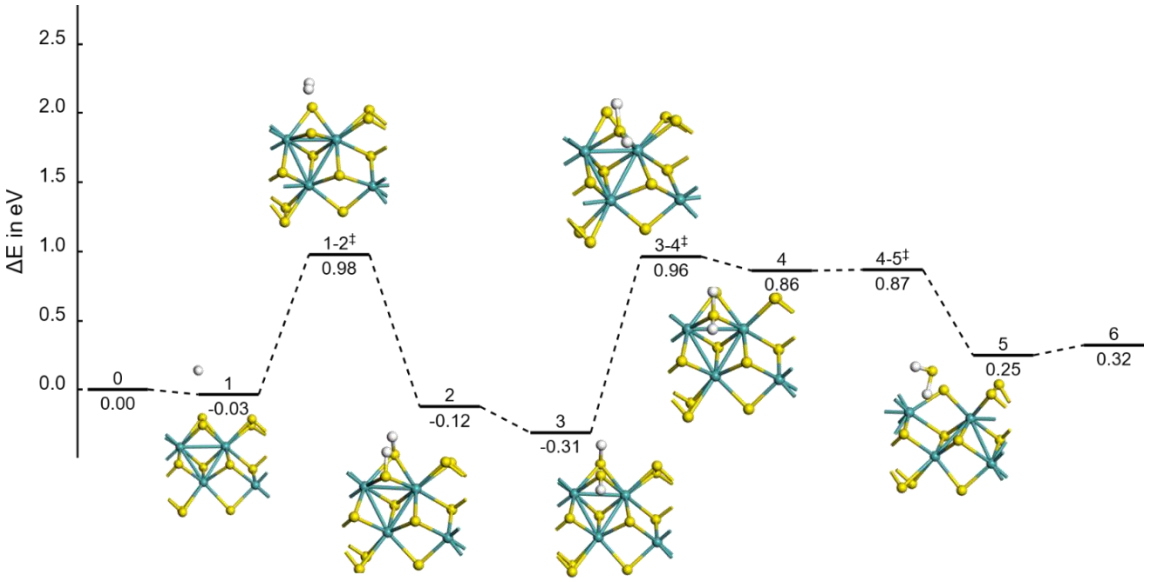

Figure S36. Free energy profile of S removal from bridging-S_2 of periodic-Mo_4S_{11}.

12. Frequency analysis

Table S2. Transition state frequencies and their respective SH-OH, HH bond lengths with corresponding TS indicator.

TS Frequencies (cm^{-1})	SH bond (Å)	OH bond (Å)	OH bond (Å)	SH bond (Å)	HH bond (Å)	TS-indicator
O/S exchanges for trimer						
761	1.61	1.25				br(1-2)
783	1.51	1.36				br(4-5)
572	1.62	1.23				t (1-2)
1468	2.23	1.28				int-bi(1-2)
963	1.49	1.46				Int-tri(1-2)
1511		1.33	1.43			Int-tri(2-3)
452	1.48	1.5				Int-tri(4-5)
S removals for trimer						
645	1.73			1.75	1.07	A(1-2)
877	1.44			2.01		A(3-4)
1108	1.58			1.63	1.08	B(1-2)
1000	1.71			1.73		B(3-4)
691	1.70			1.71	0.91	C(1-2)
890	1.69			1.65		C(3-4)
O removals for trimer						
635	1.97	1.63			0.80	D(1-2)
1036	1.99	1.67				D(3-4)
215	1.82	1.28			0.97	E(1-2)
1286	1.41	1.59				E(2-3)
902	1.52	1.404				F(1-2)
688	1.47	1.46				F(4-5)
O/S exchanges for monomer						
1029	1.61	1.25				G(1-2)
1250	1.72	1.31				G(2-3)
1001	1.55	1.34				H(1-2)
1318	1.89	1.28				H(2-3)

Table S3. Vibrational modes of various intermediates of oxides to oxysulfide reduction.

Vibrational modes	Mo_3O_9	$Mo_3O_6S_3$		$Mo_3O_3S_6$		Mo_3S_9	
		Path-1	Path-2	Path-1	Path-2	Path-1	Path-2
Alumina Modes	652, 636, 578, 561, 540, 539, 514, 495, 480, 475, 465, 452, 446, 435, 433, 410, 310, 291, 281, 265, 258, 246	637, 573, 560, 546, 532, 484, 478, 469, 455, 447, 434, 426, 420, 393, 389, 383, 361, 344, 336, 311, 299, 292, 265, 249	704, 680, 648, 617, 580, 572, 536, 533, 508 490, 481, 467, 448, 440, 425, 421, 400, 386, 368, 332, 318, 309	651, 574, 510, 497, 478, 471, 448, 442, 427, 412, 408, 400, 383, 367, 348, 305, 291, 282, 257,	667, 578, 547, 513, 480, 474, 467, 464, 451, 450, 435, 420, 409, 406, 289, 268, 262,	639, 584, 564, 490, 486, 473, 471, 448, 444, 439, 436, 404, 397, 392, 373, 364, 359, 353, 314, 293, 284, 257,	638, 573, 562, 480, 477, 465, 446, 442, 438, 436, 425, 399, 388, 382, 372, 366, 355, 315, 311, 303, 297, 283, 266, 256,
Mo-O_t	991, 989,	978	982, 970	--	970		
Mo-$O_{int\ (bi)}$	894, 866, 835, 825,	868, 831, 822, 799	839, 831,	874, 806,	813		
Mo-O_{surf}	816	755	704, 680, 648	738	702,	684	680,
Mo-$O_{int\ (tri)}$	715, 625	645	680, 648	692	687		
Mo-(O-Al)	578, 557, 544, 539, 514, 495, 480, 475, 466, 435, 352,	552, 532, 530, 511, 497, 455, 444, 434, 426, 420, 393, 383, 361, 344, 314,	580, 536, 533, 517, 508, 421, 368, 318, 309,	577, 556, 539, 497, 336, 319 , 251	575, 554, 547, 336, 316,		

	335,						
Mo-O-Mo	787, 715, 652, 636, 557, 422, 410, 398, 381, 368, 363, 352, 326, 291, 274, 281, 265, 258, 246, 227	831, 799, 511, 497, 478, 447, 420, 389, 361, 344, 265, 249, 233, 200	730, 648, 617, 533, 490, 440, 425, 347, 332, 318	548,	553, 501		
Mo-S_t		573	461,	564, 560,	568	567, 559, 520, 495 (w-int-Al)	564, 559, 504(w-int-Al)
Mo-S-Mo		511, 497, 469, 420, 333, 311, 265, 249,	519, 508, 478, 318,	471, 467, 459, 448, 383, 375, 368, 358, 356, 348, 333, 326, 245, 235, 217	494, 467, 464, 388, 377, 363, 353, 347, 322, 311, 238, 240, 238, 219	483, 473, 471, 436, 428, 413, 404, 397, 379, 373, 364, 359, 353, 341, 294, 247, 243, 226	491, 467, 450, 438, 399, 382, 378, 372, 366, 356, 355, 325, 315, 311, 303, 246, 236,
Mo-S_2				471, 467,	543	486	540

Table S 4. ΔE and ΔG of oxides, oxysulfides, and sulfides for their respective steps.

Step	ΔE (ΔG)									
	Mo_3O_9	$Mo_3O_7S_2$	$Mo_3O_4S_5$	$Mo_3O_2S_7$	Mo_3OS_6	Mo_3S_9	Mo_3S_8	Mo_3S_7	$Mo_3O_3S_6$	$Mo_3O_2S_6$
Adsorption of H_2S or H_2	-0.48 (0.55)	-0.34 (0.79)	-0.49 (0.43)	-0.67 (0.37)	-0.28 (1.04)	-0.04 (0.44)	-0.04 (0.48)	-0.03 (0.45)	-0.12 (0.40)	-0.14 (0.38)
H_2S / H_2 dissociation	0.59 (1.19)	0.13 (0.97)	1.42 (1.81)	0.94 (0.80)	0.33 (1.41)	1.17 (1.87)	0.95 (1.83)	0.46 (1.36)	1.03 (1.85)	1.08 (1.91)
Proton transfer	0.55 (1.14)	0.79 (1.62)	1.05 (1.70)	1.22 (1.66)	1.37 (1.96)	0.90 (1.74)	1.35 (2.16)	0.63 (1.49)	1.87 (1.17)	0.48 (1.05)
Water / H_2S desorption	0.23 (0.77)	0.67 (1.22)	0.52 (1.55)	1.50 (1.93)	0.37 (0.72)	0.90 (1.74)	0.92 (1.68)	0.1 (0.88)	0.88 (0.60)	0.87 (1.19)
Reconstruction				2.20 (1.70)						1.37 (1.14)

References

[1] C. Arrouvel, H. Toulhoat, M. Breysse, P. Raybaud, Effects of P_{H2O}, P_{H2S}, P_{H2} on the surface properties of anatase-TiO_2 and γ-Al_2O_3: a DFT study, J. Catal. 226 (2004) 260–272.

[2] M. Digne, P. Sautet, P. Raybaud, P. Euzen, H. Toulhoat, Hydroxyl Groups on γ-Alumina Surfaces, J. Catal. 211 (2002) 1–5.

[3] Cartwright, H. Molecular Thermodynamics. By Donald A. McQuarrie and John D. Simon. (1999) University Science Books, USA. 672 pp.

[4] J. Handzlik, P. Sautet, Structure of Isolated Molybdenum(VI) Oxide Species on γ-Alumina: A Periodic Density Functional Theory Study, J. Phys. Chem. C 112 (2008) 14456–14463.

[5] J. Handzlik, P. Sautet, Structure of Dimeric Molybdenum(VI) Oxide Species on γ-Alumina: A Periodic Density Functional Theory Study, J. Phys. Chem. C 114 (2010) 19406–19414.

[6] A. Rochet, B. Baubet, V. Moizan, E. Devers, A. Hugon, C. Pichon, E. Payen, V. Briois, Intermediate Species Revealed during Sulfidation of Bimetallic Hydrotreating Catalyst, J. Phys. Chem. C 121 (2017) 18544–18556.

[7] R.G. Leliveld, A.J. van Dillen, J.W. Geus, D.C. Koningsberger, The Sulfidation of γ-Alumina and Titania Supported (Cobalt)Molybdenum Oxide Catalysts Monitored by EXAFS, J. Catal. 171 (1997) 115–129.

[8] A. Rochet, B. Baubet, V. Moizan, C. Pichon, V. Briois, Co-K and Mo-K edges Quick-XAS study of the sulphidation properties of Mo/Al_2O_3 and CoMo/Al_2O_3 catalysts, C. R. Chim. 19 (2016) 1337–1351.

[9] A. Rochet, B. Baubet, V. Moizan, E. Devers, A. Hugon, C. Pichon, E. Payen, V. Briois, Influence of the Preparation Conditions of Oxidic NiMo/Al_2O_3 Catalysts on the Sulfidation Ability: A Quick-XAS and Raman Spectroscopic Study, J. Phys. Chem. C 119 (2015) 23928–23942.

[10] P. Sarrazin, S. Kasztelan, N. Zanier-Szydlowski, J.P. Bonnelle, J. Grimblot, Interaction of oxomolybdenum species with γ-alumina and γ-alumina modified by silicon. The silica/γ-alumina system, J. Phys. Chem. 97 (1993) 5947–5953.

[11] C. Arrouvel, M. Breysse, H. Toulhoat, P. Raybaud, A density functional theory comparison of anatase (TiO_2)- and γ-Al_2O_3-supported MoS_2 catalysts, J. Catal. 232 (2005) 161–178.